Electrosprayed mesoporous particles for improved aqueous solubility of a poorly water soluble anticancer agent: *in vitro* and *ex vivo* evaluation

Elshaimaa Sayed[1,2], Christina Karavasili[3], Ketan Ruparelia[1], Rita Haj-Ahmad[1], Georgia Charalambopoulou[4], Theodore Steriotis[4], Dimitra Giasafaki[4], Paul Cox[5], Neenu Singh[6], Lefki-Pavlina N. Giassafaki[3], Aggeliki Mpenekou[3], Catherine K. Markopoulou[3], Ioannis S. Vizirianakis[3], Ming-Wei Chang[7,8], Dimitrios G. Fatouros[3,*], Zeeshan Ahmad[1,*]

[1]Leicester School of Pharmacy, De Montfort University, Leicester, LE1 9BH, UK,

[2]Department of Pharmaceutics, Faculty of Pharmacy, Minia University, Minia, Egypt.

[3]Department of Pharmacy, Aristotle University of Thessaloniki. GR-54124 Thessaloniki, Greece

[4]National Center for Scientific Research "Demokritos", 15341 Agia Paraskevi Attikis, Greece

[5]School of Pharmacy and Biomedical Sciences and Institute of Biomedical and Biomolecular Sciences, University of Portsmouth, Portsmouth, PO1 2DT, UK

[6]Faculty of Health and Life Sciences, School of Allied Health Sciences, De Montfort University, The Gateway, Leicester LE1 9BH, UK

[7]College of Biomedical Engineering and Instrument Science, Zhejiang University, Hangzhou 310027, China

[8]Zhejiang Provincial Key Laboratory of Cardio-Cerebral Vascular Detection Technology and Medicinal Effectiveness Appraisal, Zhejiang University, Hangzhou 310027, China

Corresponding authors: Dimitrios G.Fatouros e-mail: dfatouro@pharm.auth.gr, Zeeshan Ahmad e-mail: zahmad@dmu.ac.uk

Abstract

Encapsulation of poorly water-soluble drugs into mesoporous materials (e.g. silica) has evolved as a favorable strategy to improve drug solubility and bioavailability. Several techniques (e.g. spray drying, solvent evaporation, microwave irradiation) have been utilized for the encapsulation of active pharmaceutical ingredients (APIs) into inorganic porous matrices. In the present work, a novel chalcone (KAZ3) with anticancer properties was successfully synthesized by Claisen-Schmidt condensation. KAZ3 was loaded into mesoporous (SBA-15 and MCM-41) and non-porous (fumed silica, FS) materials *via* two techniques; electrohydrodynamic atomization (EHDA) and solvent impregnation. The effect of both loading methods on the physicochemical properties of the particles (e.g. size, charge, entrapment efficiency, crystallinity, dissolution and permeability) was investigated. Results indicated that EHDA technique can load the active in a complete amorphous form within the pores of the silica particles. In contrast, reduced crystallinity (~79%) was obtained for the solvent impregnated formulations. EHDA engineered formulations significantly improved drug dissolution up to 30-fold, compared to the crystalline drug. *Ex vivo* studies showed EHDA formulations to exhibit higher permeability across rat intestine than their solvent impregnated counterparts. Cytocompatibility studies on Caco-2 cells demonstrated moderate toxicity at high concentrations of the anticancer agent. The findings of the present study clearly show the immense potential of EHDA as a loading technique for mesoporous materials to produce poorly water-soluble API carriers of high payload at ambient conditions. Furthermore, the scale up potential in EHDA technologies indicate a viable route to enhance drug encapsulation and dissolution rate of loaded porous inorganic materials.

KEYWORDS: Mesoporous silica, chalcones, electrohydrodynamic atomization, electrospraying, poor solubility, *ex vivo*, molecular modelling, cytocompatibility

1. Introduction

Cancer is a deleterious disease that accounts for a high annual global mortality rate. Progress in the development of novel cancer therapies is timely and rapid, however has not resulted in a satisfactory decrease in cancer related morbidity [1]. Conventional chemotherapeutic agents encounter numerous issues such as off-target cytotoxicity, poor water solubility, limited permeability and high clearance. As a result, the bioavailability of the API remains poor not achieving sufficient concentration at the tumour site [2]. Therefore, the need to develop appropriate anticancer agents and suitable drug delivery systems for efficient cancer therapy is urgent. Chalcones, either naturally occurring or their synthetic analogues, are a group of biologically active compounds with anti-inflammatory, anti-mutagenic, antipyretic, analgesic, and antioxidant activities [1,3]. Interestingly, they are emerging in anticancer drug discovery and are attracting a significant attention from drug designers [4]. They can exert cytotoxic, anti-mitotic, anti-proliferative properties via molecular alteration such as apoptosis induction, mitochondrial damage, kinases and tubulin inhibition, and angiogenesis inhibition. [1,3-6]. Chalcones possessing lower hydroxylation and higher methoxylation are more efficient in inducing apoptosis and inhibiting proliferation [6], and especially their substituted derivatives are known to minimally interact with biological molecules compared to the conventional clinically used drugs, thus inducing a lower risk of genotoxicity and mutagenicity [4]. Although these biological properties offer them an exciting prospect, their poor aqueous solubility has restricted their medical and pharmaceutical applications [7].

Various strategies have been explored to enhance drug solubility [8-14] among which solid dispersions [11,13], nanosizing [15], inclusion complexes [16], spray drying [17], electrohydrodynamic atomization (EHDA) [18] and loading into mesoporous materials

[19-23]. Utilising amorphous forms of active pharmaceutical ingredients (API) has also gathered appreciable pace over the last decade due to their high dissolution rate and bioavailability [24].

Mesoporous silica materials (pore size 2 - 50 nm) have been explored as targeted [2,25] responsive [26] and controlled [27,28] drug delivery systems, because of their favourable features, such as a stable ordered porous network, accessible silanol groups, high surface area as well as uniform and tuneable pore and particle size [29]. They are considered as promising API carriers which improve the dissolution rate and oral bioavailability of poorly water-soluble drugs [21,30] by drug amorphization [19]. Previous studies have utilized mesoporous silica to improve the dissolution of telmisartan [10], ibuprofen [20], fenofibrate [23], itraconazole [21], piroxicam [19], camptothecin [31] and paclitaxel [32]. Numerous studies clearly indicate that the drug loading method on mesoporous silica materials has a substantial impact on the resulting properties of the active such as on their stability, amorphous state, loading efficiency, dissolution rate and bioavailability [8,23,33]. EHDA (also termed electro-spraying) is considered a versatile and flexible technique for the preparation of polymeric nano- and micro-particulate materials with high API encapsulation efficiency and narrow particle size distribution and has been explored for a wide range of pharmaceutical and biomedical applications [9,18,34,35].

In the present work, a novel chalcone (KAZ3) with high degree of methoxylation was successfully synthesized using the Claisen-Schmidt condensation method. KAZ3 is a poorly soluble compound therefore a good candidate for assessing the dissolution enhancing effect of electrospraying technique utilizing silica matrices as the drug carrier. KAZ3 was loaded into mesoporous (SBA-15, MCM-41) and non-porous (fumed silica) particles using the solvent impregnation and EHDA techniques. Among

different mesoporous carriers, the hexagonally ordered mesostructured SBA-15 and MCM-41 are the most investigated mesoporous materials in literature, because of the high stability of their mesostructures and their convenient method of synthesis [21,29,36]. Although both materials are made of amorphous SiO_4 tetrahedra and have hexagonally arranged arrays of pores [29], they differ in pore geometry. SBA-15 possesses circular pore geometry, a wider pore size (5-10 nm) and a thicker wall, compared to MCM-41 which is characterized by a hexagonal pore geometry and pores in the range of 2-5 nm [36,37].

In the present study, the drug loaded mesoporous formulations were developed after process optimization (jet mapping) and were characterized in terms of particle size and morphology (scanning electron microscopy, laser diffraction), contact angle and drug crystallinity (differential scanning calorimetry, Fourier Transform Infrared Spectroscopy, Powder X-ray diffraction). The dissolution and permeability profiles of the drug loaded mesoporous formulations were assessed *in vitro* in phosphate buffer solution pH 7.4 (PBS) and *ex vivo* using the non-everted gut sac method, respectively. Cytotoxicity evaluation of the mesoporous formulations was conducted on intestinal epithelial cells (Caco-2 cells).

To the best of our knowledge, this is the first thorough study on EHDA engineering for direct drug loading into mesoporous materials. The potential for enhanced drug loading, increased stability of the drug in the amorphous state, ultimately displaying improved dissolution and permeability profiles is demonstrated.

2. Materials and methods

2.1 Materials

3′,4′,5′-Trimethoxyacetophenone, 4-Anisaldehyde, sodium hydroxide, methanol, ethyl acetate, petroleum ether and anhydrous magnesium sulphate were purchased from Alfa Aesar (Lancashire, UK) and Fisher Scientific (Loughborough, UK). Ethanol, Acetone, Pluronic P123, tetraethylorthosilicate (TEOS 98%) ammonia (NH3 25%) and cetylmethylammonium bromide (CTAB) were supplied from Sigma-Aldrich Chemical Company (Dorset, UK). All reagents were of the analytical grade. Non-porous fumed silica AEROSIL® 130 was obtained from Evonik Industries AG.

2.2 Synthesis of (E)-3-(4-methoxyphenyl)-1-(3,4,5-trimethoxyphenyl)-prop-2-en-1-one (KAZ3)

The Claisen-Schmidt condensation reaction (Supplementary Material [SM], scheme S1) was adopted for chalcone synthesis [38]. Briefly, sodium hydroxide solution (50 % w/v, 66.7 mmoles, 5.3 mL) was added to a stirred solution of the 3′,4′,5′-Trimethoxyacetophenone (0.908g, 6.67 mmoles) and 4-anisaldehyde (1.4g, 6.67 mmoles) in methanol (30 mL). The resulting mixture was stirred at room temperature and sequentially monitored by TLC (ethyl acetate/petroleum ether (3:7) upon the completion of the reaction. The reaction was quenched with distilled water (30 mL) and extracted with ethyl acetate (3 x 30 mL). The combined organic extract was washed with brine (50 mL), dried with anhydrous magnesium sulphate and the solvent was removed under vacuum. The crude product was recrystallized from ethanol to afford a yellow solid of 1.96 g (89 % yield). The structure of the formed chalcone was confirmed using an array of different analytical methods including nuclear magnetic resonance

(NMR), mass spectroscopy (MS), Fourier transform infrared spectroscopy (FTIR) and thin layer chromatography (TLC). (SM, section 1.2)

2.3 Molecular simulations

Molecular dynamics (MD) calculations were performed using the program Materials Studio, in order to screen whether microporous or mesoporous materials would be better carrier candidates of KAZ3 [39]. A single drug molecule was placed inside the framework of each of the two host structures (microporous zeolites and mesoporous silica). Periodic boundary conditions were applied, and the simulations were performed at a temperature of 310K. The universal forcefield was used with charges calculated via the QEq methodology. Each simulation was run for a total of 4 million steps with a time-step of 1 x 10-15 s.

2.4 Synthesis and characterization of mesoporous silica host.

2.4.1 Synthesis of SBA-15 particles

The SBA-15 mesoporous particles were prepared according to a well-established method [40], using triblock copolymer EO20PO70EO20 (Pluronic P123) as the surfactant and tetraethylorthosilicate (TEOS 98 %) as the silica source. The surfactant was initially dissolved in an acidic (HCl) aqueous solution at 35 °C, followed by the addition of TEOS under stirring at 35 °C for 2h. The mixture was transferred into an autoclave, maintained at 35 °C for 20 h (without stirring) and subsequently aged at 90 °C for 24 h. The solid product was recovered by filtration without washing and air-dried at 80 °C. The removal of the surfactant took place through calcination at 550 °C for 6 h with a heating rate of 1 °C /min.

176 2.4.2. Synthesis of MCM-41 particles

177 The MCM-41 particles were synthesized under basic conditions through the hydrolysis
178 of TEOS in a water/ammonia (NH_3 25 % w/w) mixture containing
179 cetylmethylammonium bromide (CTAB) as the surfactant agent [41]. The mixture was
180 stirred for 30 min and subsequently heat-treated at 80 °C for 96 h in an autoclave. The
181 final product was retrieved after filtering, rinsing with cold ethanol and air-drying,
182 followed by calcination at 550 °C for 5 h (heating rate: 2 °C/min). Geometry and pore
183 volume of the produced mesoporous silica were characterized using small angle X-ray
184 scattering (SAXS) and N_2 adsorption-desorption isotherms (SM, section 1.3)

185

186 2.5 Drug loading methods

187 2.5.1. Solvent impregnation method

188 SBA-15, MCM-41 or FS particles (6 mg/mL) were dispersed in acetone or ethanol drug
189 solutions (2 mg/mL) using a water bath sonicator for 15 minutes. The resulting
190 suspensions (target drug loading was set at 25 % w/w, SM, Section 2.3) were
191 magnetically stirred overnight in screw-capped vials. An aliquot of 1 mL of the
192 dispersion was centrifuged and drug was quantified in the supernatant with UV
193 spectrophotometry. The cap was removed in order to allow evaporation of solvents
194 whilst stirring to obtain KAZ3 loaded mesoporous silica particles in a solidified form.

195

196 2.5.2. Electrospraying method

197 Identical procedures were used to prepare dispersions of mesoporous or non-porous
198 silica in drug solutions. Five millilitres of each dispersion were loaded into a syringe
199 which was connected to a stainless steel conductive needle using silicone tubing. A
200 syringe pump (world precision instruments, UK) was used to control the infusion rate

(25 µL/min) of suspensions through the needle. An electric field (16 -17.5 kV) was applied to the metallic needle using a high voltage power supply (Glassman high voltage supply, UK). The deposited particles were collected for 3.5 h onto a glass substrate. It is worth mentioning that increasing silica particle concentration of the suspension above 12 mg/mL resulted in blockage of the needle nozzle. For scaling up, the electrospraying could be performed by adopting a multiple nozzle system, a nozzle-less system or by increasing the nozzle diameter. The drug content of the sprayed product was quantified with UV spectrophotometry. Accurately weighted amounts of each sample were dispersed in acetone and sonicated for 20 minutes. The suspensions were then centrifuged, and the drug content was quantified in the supernatant solutions.

2.6 Drug loading efficiency

The composition of the drug-loaded samples, loading methods and entrapment efficiencies using UV spectrophotometry are presented in Table 1. The entrapment efficiency (EE %) was calculated according to equation 1.

$$EE\% = \frac{Actual\ amount\ of\ drug\ present\ in\ samples}{Expected\ theoretical\ amount\ of\ drug}\ x\ 100 \qquad [1]$$

2.7 Jet mapping

Jetting maps were established by gradually increasing both flow rate (1-100 µL/min) and applied voltages (0 - 20 kV) in order to optimize the electrospraying process. For map construction, suspensions of silica particles (MCM-41, SBA-15 and FS) in acetone and ethanol were used. The jetting behaviour was monitored using a camera (GX CAM HiCHROME-MET, GT vision, Suffolk, UK) and images of jetting modes were obtained.

2.8 Scanning electron microscopy (SEM) studies

The morphology of loaded and unloaded silica particles was investigated by means of scanning electron microscopy (SEM, Carl Zeiss EVO HD-15, Oberkochen, Germany). Particles were mounted onto double adhesive layer on an aluminium stub. The samples were gold-coated using ion sputtering device (Edwards S150B, West Sussex, UK) and scanned at an accelerating voltage of 10 kV.

2.9 Thermal gravimetric analysis (TGA)

Thermal gravimetric analysis of pristine silica materials, physical mixtures (drug/silica) and the drug loaded samples was performed using a TGA analyzer (Perkin Elmer, Pyris). Samples (~5 mg) were placed in porcelain pans and were heated in nitrogen gas over the range 20-800 °C with a heating rate of 10 °C/min. Entrapment efficiency was calculated using equation 2.

$$EE\% = \frac{\%Wt\ loss\ of\ drug\ loaded\ samples\ from(\ 100-800℃) - \%\ wt\ loss\ of\ silica\ from\ (100-800℃)}{Theoretical\ drug\ content\ \%} \quad [2]$$

2.10 Differential scanning calorimetry (DSC)

The thermograms of the KAZ3, MCM-41, SBA-15, FS, physical mixtures and the drug loaded samples were obtained on a PerkinElmer differential scanning calorimeter (Shelton, USA). The samples (~5 mg) were loaded in aluminum pans and were heated from 20 - 400 °C at a rate of 10 °C/min under a nitrogen stream at a flow rate of 20 mL/min. The percentage of crystallinity of the drug loaded samples was calculated using the enthalpy of melting according to equation 3 [42]:

$$\%\ \text{Crystallinity} = \frac{\Delta Hm}{\Delta Hm^{\circ}}\ \text{x}\ 100\% \quad [3]$$

Where ΔH_m is the melting enthalpy of the drug loaded formulations, ΔH_{m^0} is the melting enthalpy of a fully crystalline reference material (100 % crystallinity); in the

current study, the physical mixture of each silica type with equivalent drug quantity was considered as the reference material.

2.11 Powder X-ray diffraction (PXRD)

The crystalline state of the raw materials and the drug loaded samples was investigated by PXRD analysis on a Bruker D8-Advance diffractometer (USA) using Cu $K\alpha_1$ radiation (λ = 1.54 Å) over the 2θ range from 8º to 35º and a step size of 0.03º.

2.12 Contact angle measurements

Water contact angle on drug, unloaded and drug loaded mesoporous silicas were measured using a sessile drop profile by an optical tensiometer (Theta Lite, Biolin Scientific, Sweden). A water drop of approximately 5µL of each sample was deposited using a liquid manual dispenser (Hamilton syringe with a 22 gauge needle) on a smooth homogenous surface. The images of the drop were recorded at different time intervals. The contact angles were measured on both sides of the sessile drop and the average was taken as the result.

2.13 *In vitro* release studies

Pure drug or drug-loaded formulations were suspended in 2 mL of phosphate buffer saline (PBS) solution in capped Eppendorf tubes. *In vitro* release studies were conducted in a shaking water bath (60 rpm) at 37 °C under sink conditions. At different time intervals, the Eppendorfs were centrifuged and 1.5 mL samples were withdrawn and replaced with the same volume of fresh PBS. The drug content in each sample was quantified with UV spectrophotometry at 350 nm. Release experiments were carried out in triplicate and averaged results were reported.

2.14 *Ex vivo* intestinal permeability studies

Ex vivo intestinal permeation of KAZ3 (250 μg) from suspensions and the KAZ3 loaded silica particle formulations, containing equivalent amount of drug, was evaluated using the non-everted gut sac method [43]. Male Wistar rats were fasted overnight with free access to water. The animals were euthanized and the small intestine was excised by cutting from the upper end of the duodenum to the lower end of the ileum. Intestine was thoroughly washed with cold Krebs-Ringer solution using a syringe with a blunt end. The non-everted tissue was cut into 5 cm segments and tied with silk suture from the one end. After filling with 0.5 mL of either KAZ3 suspension or KAZ3 loaded particle suspensions (equivalent to 0.25 mg KAZ3) both intestinal ends were knotted, and the formed sacs were immersed in 200 mL oxygenated Krebs-Ringer solution pH 7.4 at 37 ^{o}C. Aliquots of 1 mL were withdrawn at 30, 60, 90 and 120 min and replenished with an equal volume of fresh pre-warmed buffer solution. Samples were filtered through 0.22 μm membrane syringe filters and the amount of drug permeated was quantified with HPLC analysis (SM, section 1.6). Experiments were conducted in accordance with the European Community guidelines for the use of experimental animals.

The amount of drug which permeated across the intestine was determined using equation 4.

$$\text{Apparent permeability } (\mu g/cm^2) = \frac{\text{concentration x volume}}{\text{mucosal surface area}} \quad [4]$$

The mucosal surface area was calculated according to equation 5, considering the intestine a cylinder.

$$\text{Mucosal surface area } (cm^2) = \pi \times diameter \times \text{ intestine length} \quad [5]$$

2.15 Cytocompatibility studies

Caco-2 cells (colon adenocarcinoma human cell line) were cultured in Dulbecco's modified Eagles Medium (DMEM) supplemented with 10% fetal bovine serum (FBS) and 100 U/mL penicillin, and 100 μg/mL streptomycin and maintained at 37 ºC in a humidified atmosphere (95% relative humidity) containing 5% v/v CO_2. In stock cultures, cells were subcultured by trypsinization in tissue culture flasks every 48 - 72 hours. In the experiments described, Caco-2 cells were used at passages 40 - 45.

2.16 *In vitro* cytotoxicity assay

The cytotoxicity effect of pure KAZ3 and the drug loaded MCM-41, SBA-15 and FS materials on Caco-2 cells was evaluated by the MTT (3-(4,5-dimethylthiazol-2-yl)-2,5-diphenyltetrazolium bromide) colorimetric assay (Trevingen®) [44,45] in a time- and concentration-dependent manner. Caco-2 cells were seeded in 96-well plates at an initial density of 10^4 cells/well and were left overnight to attach. The cells were then exposed to KAZ3 at increasing concentrations (0.1 μM - 100 μM) and the drug loaded MCM-41, SBA-15 and FS carriers at two different concentrations (0.1 mg/mL and 1 mg/mL) for 4 h, 24 h and 48 h. Untreated cells were considered as negative control, whereas cells treated with 1 % v/v Triton X-100 were used as positive control. After the specified time-points, 10 μL of the MTT reagent (5 mg/mL) were added in each well and the 96-well plate was incubated for a further 1 h at 37 ºC in a humidified atmosphere. The medium was then replaced with 100 μL DMSO to allow dissolution of the formed formazan crystals and the absorbance of the colored, solubilized product was read at 590 nm using an ELISA microplate reader. Percent cell viability was calculated according to equation 6.

Relative cell viability (%) = $(OD_{\text{treated cells}}-OD_{\text{blank}})/(OD_{\text{control cells}}-OD_{\text{blank}}) \times 100$. [6]

Results are expressed as the mean value ± standard deviation (S.D.) of three independent experiments.

3. Results and Discussion

3.1. KAZ3 Synthesis and characterization

The chemical structure of the synthesised chalcone (KAZ3) is shown in Figure S1. The drug was synthesized to afford a decorated aromatic ring with 4-methoxyphenyl (B-ring) and 3,4,5-trimethoxyphenyl (A-ring). Methoxylation of the aromatic groups intended to increase the antiproliferative activity of the drug [6]. In addition, this decoration aimed to decrease the reactivity of α, β-unsaturated carbonyl group thus decreasing their possible interactions with biological molecules and therefore the potential of adverse effects [7]. The purity of the product was determined by TLC and elemental analysis. The product was also characterized by proton & carbon-13 NMR, infrared spectroscopy and mass spectrometry (SM, Figure S2).

3.2. Molecular simulation studies

The simulations were used to investigate the diffusion properties of KAZ3 inside a typical microporous zeolite (BEA) and a mesoporous material (MCM-41) in order to determine the most pertinent carrier for loading and release of KAZ3, prior to carrying out experimental studies. MCM-41 was chosen to be a model for mesoporous silica as it is difficult run MD studies for SBA-15 due to its amorphous character since the exact nature of the structure is not well-defined. Snapshots of the position of KAZ3 during the course of the simulation show that the molecule does not diffuse through the microporous channels of the BEA structure (Figure 1A). Although the molecule fits inside the zeolite, it is unable to travel through the structure because it is too bulky to move between the intersections in the zeolite's channel system. This lack of movement

is confirmed by the calculated root-mean displacement for the molecule, which shows a flat line (Figure 1C). In contrast, the RMS displacement for the drug inside the MCM-41 framework shows a steady increase during the course of the simulation (Figure 1C). KAZ3 is easily accommodated within the larger channel system of MCM-41 (Figure 1B) and interacts with the –OH groups on the internal surface, but the interaction is insufficiently strong for it to be held tightly in place at the simulation temperature. As a result, the molecule moves slowly across the internal surface of MCM-41. The simulations suggest that mesoporous materials of this type may be relatively easy to load, and that some degree of controlled release will be observed experimentally. As a result, mesoporous materials (MCM-41 and SBA-15), rather than microporous were selected for experimental investigation.

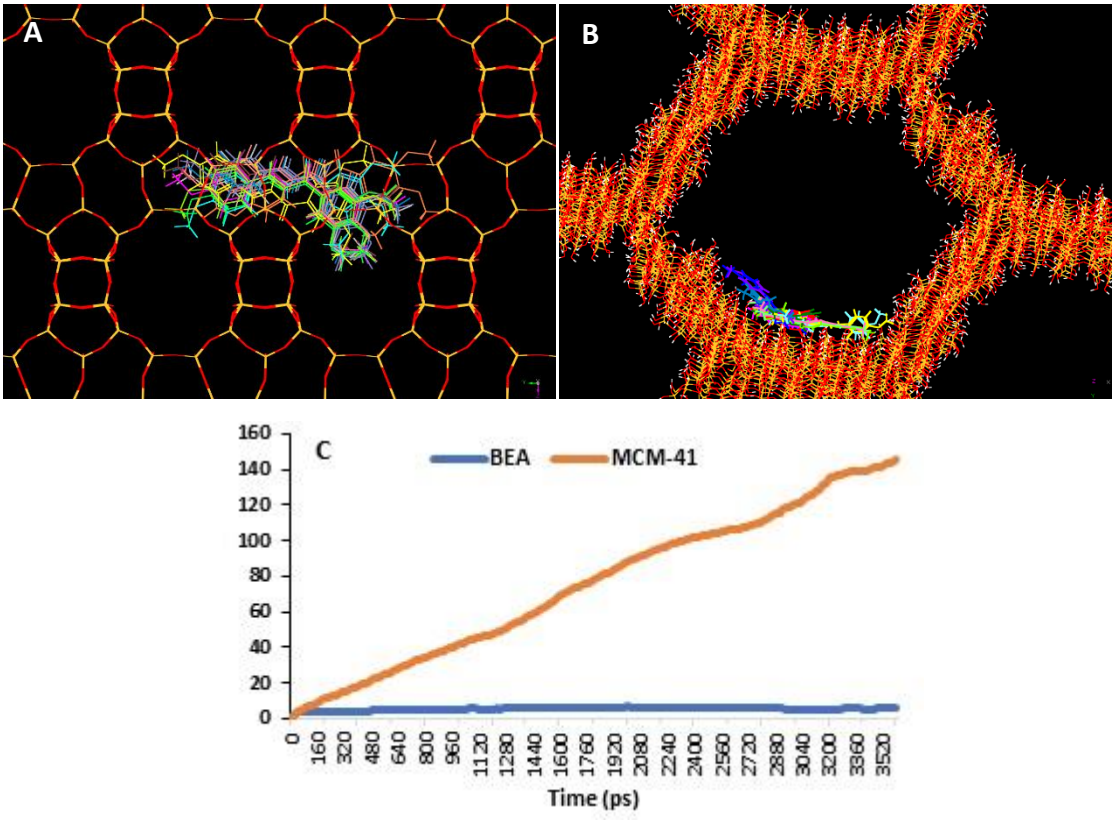

374 **Figure 1.** Snapshots showing the location of the drug molecule in **A.** BEA and **B.** MCM
375 framework every 40 ps during the simulation run. **C.** Root mean squared displacement
376 for KAZ3 in BEA and MCM-41.
377
378 3.3 Structural characterization of porous carriers
379 X-ray diffractograms (SM, Figure S3) of both mesoporous materials (SBA-15 and
380 MCM-41) exhibited the typical pattern of 2-D hexagonal space group (*p6mm*). The N_2
381 adsorption data (SI, Figure S3 and Table S1) showed that both materials depict large
382 BET areas (700-1000 m^2/g) and pore volumes (~1 cm^3/g), as well as a narrow pore size
383 distribution (PSD) with a mean pore width of 8 nm for SBA-15 and 4 nm for MCM-41.
384 MCM-41 materials are generally characterized by a pore size of 2 to 10 nm, while SBA-
385 15 exhibit larger pores between 4.6 to 30 nm [46]. For drug delivery applications, the
386 pore sizes usually range between 3 and 10 nm [28].
387
388 3.4. Jetting maps
389 Four different modes were encountered during EHDA; (i) dripping mode, (ii) unstable
390 jetting mode, (iii) stable single jet and (iv) stable multi jet. The dripping mode is
391 observed when a liquid fragment rises from the nozzle exit often without sufficient
392 applied voltage, while the stable jetting is obtained when the liquid breaks into finer
393 droplets [47]. The jetting maps for all sprayed formulations are shown in Figure 2 (A-
394 F). The jetting maps are constructed to enable the detection of a relationship between
395 the flow rate and the applied voltage; yellow regions represent the dripping mode; green
396 sections show stable jetting and the blue areas display unstable jetting states. The
397 dripping mode was attained in all sprayed formulations, generally observed when low
398 voltages were applied (0 - 10 kV). Increasing the applied voltage to >10 kV yielded

unstable jetting modes but required further increments to be balanced with flow rate (as shown in each jetting map) to ensure that stable jetting is achieved.

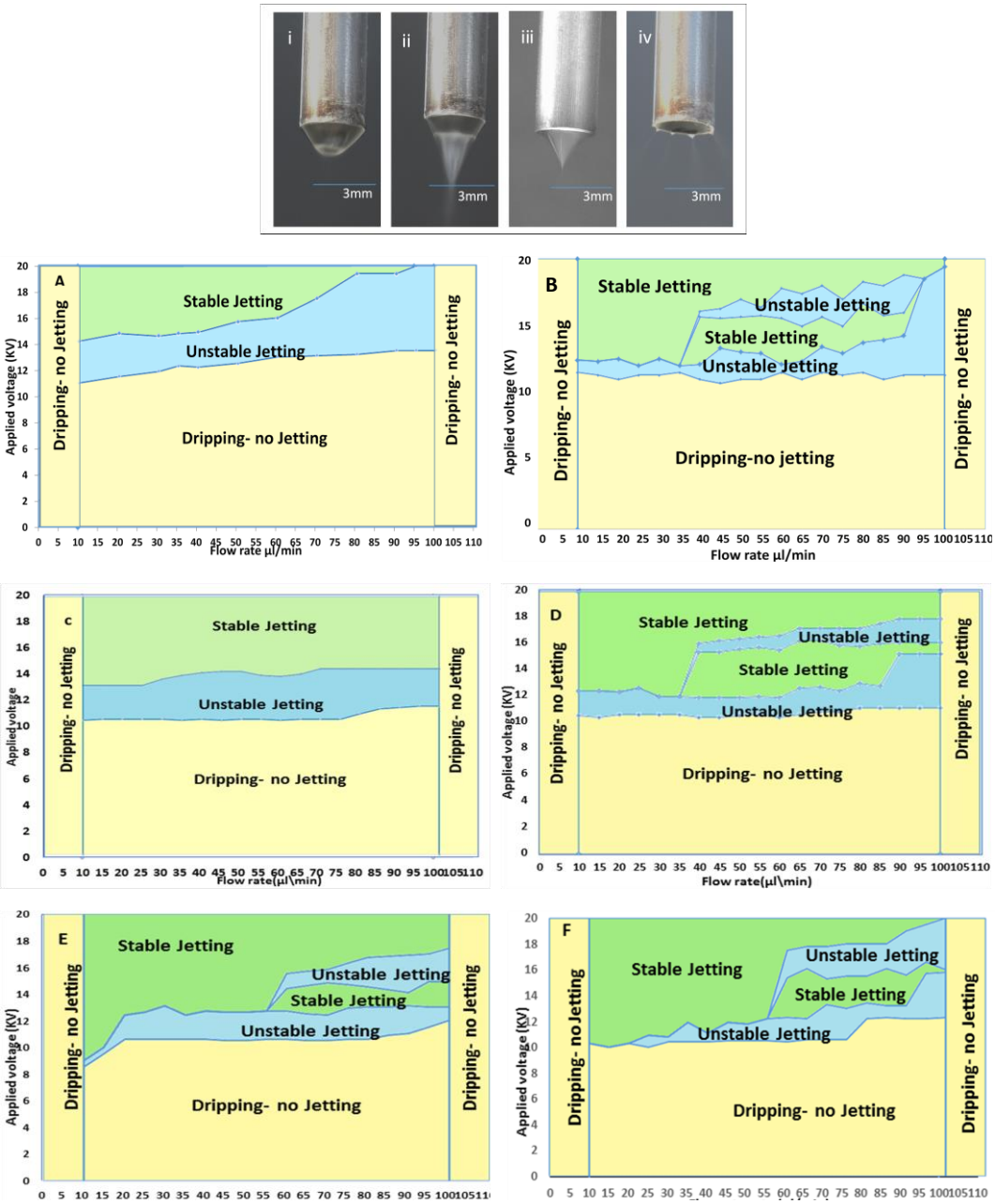

Figure 2. Jetting images i) micro-dripping ii) unstable jetting iii) stable cone jet iv) stable multi-jet and jetting maps of **A.** SBA-15 in acetone **B.** SBA-15 in ethanol **C.** MCM-41 in acetone **D.** MCM-41 in ethanol **E.** FS in acetone and **F.** FS in ethanol.

3.5. Particle morphology

SEM images of the pristine silica particles and the loaded formulations (20 kX) are shown in SM, Figure S5. Selected formulations are shown in Figure 3 at a higher magnification (40 kX) to examine the impact of drug loading on particle surface. Drug-loaded formulations prepared using solvent impregnation show rough topographical features as a result of dispersed active crystal formation on their surface (Figure 3D).

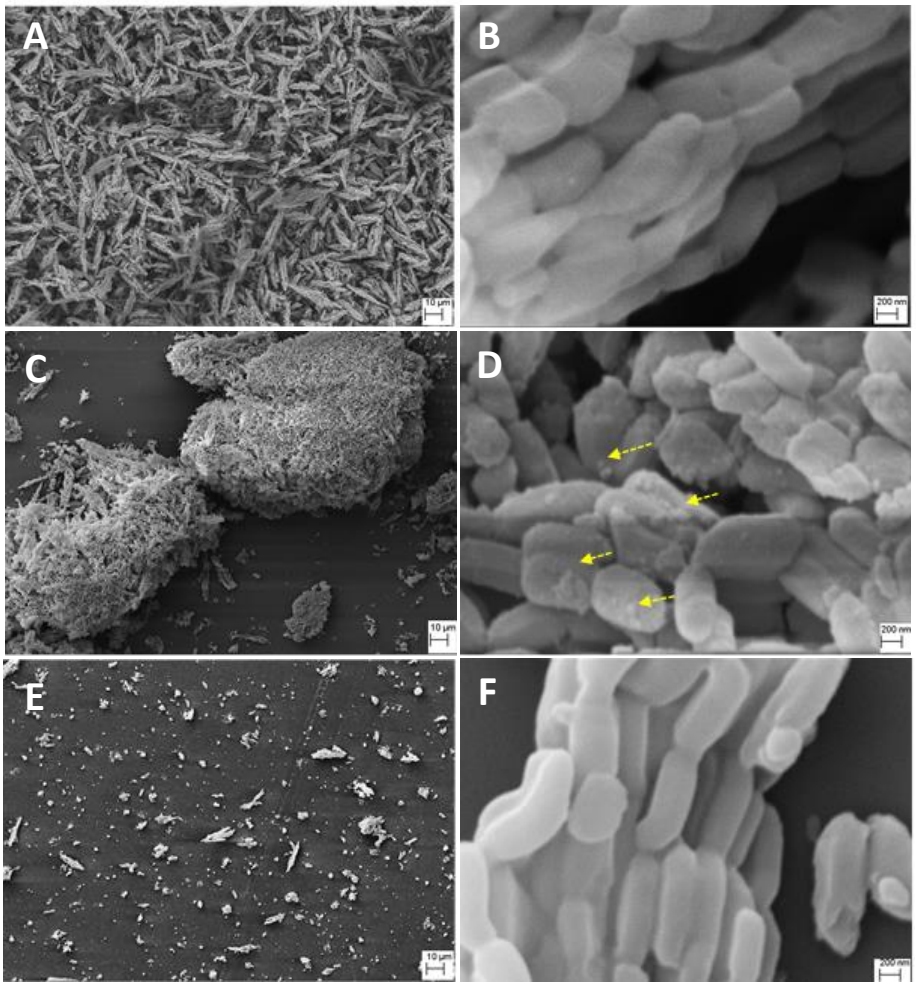

Figure 3. Scanning electron microscope images of **A.** and **B**. SBA-15 at 5 kX and 40 kX magnification, respectively. **C**. and **D**. SBA-Eth-SIM at 5 kX and 40 kX magnification, respectively. **E**. and **F**. SBA-Eth-SP at 5 kX and 40 kX magnification, respectively. SBA: SBA-15, Eth: Ethanol, SIM: solvent impregnation method and SP: electrospraying method.

In contrast, electrosprayed particles (Figure 3F) preserve particle surface morphology exhibiting smooth surfaces with little to none drug crystals present on the particle surface. This observation indicates that most drug is encapsulated within the pores of mesoporous silica. Lower magnification analysis (5 kX) revealed an aggregation tendency post drug loading. Solvent impregnated particles showed a greater tendency to aggregate during the loading process to form coarse clusters (Figure 3C), attributed to the cohesive properties of surface deposited drug crystals [8]. However, particles engineered using electrospraying appear more scattered and the presence of fused fiber-like structures is reduced (Figure 3E). During the electrospraying process mesoporous silica particles are atomized into smaller droplets favouring the disaggregation of the longer chained agglomerates into individual rod like structures.

3.6. Drug content and entrapment efficiency (EE%)

3.6.1 Determination of EE % using UV spectrophotometry

The drug loading efficiencies of all formulations are listed in Table 1. The results reveal that the loading method affects the loading efficiency of mesoporous silica particles. The loading efficiency of electrosprayed mesoporous silica was higher compared to those prepared using the solvent impregnation technique, exceeding 90.5 %. On the contrary, formulations prepared using the solvent impregnation technique showed loading efficiencies up to 35.6 %. The significant improvement in loading efficiency using EHDA is attributed to the rapid evaporation of sprayed solvent droplets, due to instabilities and bending motions which force the drug to be infiltrated inside the silica pores. Furthermore, droplets arising from the atomisation process naturally increase the surface area for drying. The choice of organic solvent also affects the loading efficiency. The loading efficiency of SBA-AC-SIM particles was higher (35.65 %)

compared to that of SBA-Eth-SIM (18.29 %), accounting for the lower polarity of acetone compared to ethanol. The more polar solvent (ethanol) favours the accommodation of large quantities of KAZ3 in solution, thus lowering the amount of drug adsorbed into pores [48]. The use of acetone for electrospraying mesoporous silica particles resulted in loading efficiencies of up to ~100 % with high intra-batch variability. In these cases, heterogeneous dispersions of the drug within the silica matrix were obtained, because of sedimentation of silica particles in the drug solution during the electrospraying process.

The pronounced effect of acetone on particle instability is further corroborated by ζ-potential measurements (SM, Table S4). The ζ-potential values of mesoporous silica particles in acetone were -9.75 mV for SBA-15 and -4.45 mV for MCM-41. On the contrary, the absolute value of ζ-potential data obtained for ethanol based mesoporous silica dispersions was higher than 30 mV for both types indicating greater stability [49]. The effect of medium viscosity is equally important for dispersion stability. The low viscosity of acetone (0.39 cP) resulted in accelerated sedimentation of silica in the organic solvent. On the contrary, the greater viscosity of ethanol (1.1 cP) led to a more stable suspension. It is well accepted that the type of silica substrate greatly influences the loading efficiency of the drug. For the solvent impregnation method, mesoporous SBA-15 displayed higher loading efficiency than MCM-41, due to the larger pore size of SBA-15 compared to MCM-41. With regard to electrosprayed formulations, both types achieved similar drug encapsulation values (EE $\geq$ 90.58%). Reduced drug loading values were obtained using non-porous FS. The drug content in nonporous FS formulations is attributed to surface drug adsorption, originating from interactions between the active compound and the surface silanol groups.

3.6.2 Determination of EE % using TGA

The thermogravimetric behaviour of silica particles before and after drug loading is shown in SM (Figure S8). The drug content of the silica formulations was determined following correction of the TG curve from water content by using the weight loss at temperature range 100 - 800 ˚C, as by this stage, all drug content had decomposed. EE's are listed in Table 1**.** The EE of solvent impregnated samples were found to be higher than those calculated spectrophotometrically. TGA was performed on dried samples, which accounts for drug deposits on the surface following complete solvent evaporation. However, calculated EE for electrosprayed samples were similar to the ones calculated using spectrophotometry. As shown in Table 1, the electrosprayed mesoporous formulations exhibited higher EE compared to those loaded using the solvent impregnation method.

3.7. XRD and DSC studies

XRD and DSC were used to characterize the physical state of the drug in the silica formulations. XRD patterns of drug loaded formulations are demonstrated in Figure 4 (A, B & C). No diffraction peaks were detected in any of the electrosprayed mesoporous formulations as compared to the pure crystalline drug or to the corresponding physical mixture, indicating the presence of the drug in the amorphous state in the mesopores of the silica, because of the fast solvent evaporation of the EHDA technique. The X-ray diffraction patterns of the solvent impregnated formulations showed characteristic peaks of the drug in the crystalline state, but with lower intensities for the acetone impregnated formulations and sharper peaks for the ethanol impregnated samples, suggesting the presence of drug precipitates on the surface of the silica particles, due to the slow solvent evaporation during this technique. XRD results

524 correlate well with the data obtained from DSC studies [Figure 4 (D, E & F)]. The
525 percentage of drug crystallinity in each formulation was determined using the drug's
526 melting enthalpies (SI, Table S5). The thermogram of the pure crystalline drug exhibits
527 a sharp endothermic melting peak at 101 °C. The thermograms of the physical mixtures
528 show a sharp peak at 98 °C. All solvent impregnated formulations showed a broadened
529 endothermic peak at 116 °C for SBA-15 formulations and at 108 °C for MCM-41
530 samples. The broadening and shift of the melting peaks suggests a reduction in drug
531 crystallinity, indicating partial amorphization [50].
532 The percentage of drug crystallinity in the solvent impregnated formulations ranged
533 between 33.18 % and 79.85 % and a higher crystallinity was detected for the ethanol
534 than the acetone impregnated formulations. No endothermic peaks were detected in the
535 thermograms of the electrosprayed formulations using ethanol (SBA-Eth-SP and
536 MCM-Eth-SP), indicating drug entrapment in the silica in the amorphous state [51].
537 The absence of drug's melting peak in the thermograms of drug loaded mesoporous
538 particles has been previously reported in several studies [8,42,51]. However,
539 electrosprayed formulations using acetone (for SBA-AC-SP and MCM-AC-SP)
540 showed a small melting peak at approximately 95 °C and drug crystallinity was
541 calculated to be 12.96 % and 14.82 %, respectively. This is justified by the
542 heterogeneous dispersion of the drug within silica, leading to crystallization of a small
543 quantity of the drug molecules. The underestimated crystallinity when using XRD is
544 most likely related to reduced diffraction intensity upon nano- sizing [18].

Table 1. Quantification of KAZ3 encapsulation efficiency (EE %) of the different formulations calculated by UV spectrophotometry and TGA.

Formulation	MS type	Loading Method	Solvent	EE (%)-UV	EE (%)-TGA			
					Silica wt. loss (%) (100 ˚C-800 ˚C)	Formulation wt. loss (%) (100 ˚C-800 ˚C)	KAZ3 content (%)	EE (%)
SBA-AC-SIM	SBA-15	Solvent impregnation	Acetone	35.65 ± 3.25	8.23	25.7	17.47	69.88
SBA-Eth-SIM	SBA-15	Solvent impregnation	Ethanol	18.29 ± 0.86	8.23	24.29	16.06	64.25
SBA-AC-SP	SBA-15	EHDA	Acetone	114.53 ± 5.25	8.23	41.29	33.06	132.26
SBA-Eth-SP	SBA-15	EHDA	Ethanol	91.79 ± 0.42	8.23	34.75	26.52	106.10
MCM-AC-SIM	MCM-41	Solvent impregnation	Acetone	28.53 ± 0.73	14.8	29.33	14.53	58.13
MCM-Eth-SIM	MCM-41	Solvent impregnation	Ethanol	15.28 ± 10.28	14.8	29.91	15.11	60.45
MCM-AC-SP	MCM-41	EHDA	Acetone	105.89 ± 5.05	14.8	41.15	26.35	105.41
MCM-Eth-SP	MCM-41	EHDA	Ethanol	90.58 ± 0.72	14.8	32.3	17.50	70.0
FS-AC-SIM	Fumed silica	Solvent impregnation	Acetone	13.14 ± 2.95	8.16	27.34	19.18	76.72
FS-Eth-SIM	Fumed silica	Solvent impregnation	Ethanol	9.48 ± 0.38	8.16	29.24	21.24	84.98
FS-AC-SP	Fumed silica	EHDA	Acetone	115.18 ± 7.68	8.16	36.72	28.72	114.89
FS-Eth-SP	Fumed silica	EHDA	Ethanol	65.35 ± 0.37	8.16	29.42	21.42	85.71

3.8. Contact angle goniometry studies

Contact angle is a macroscopic parameter which is often used to determine the interaction between liquid droplets (mostly water) and solid surfaces [52]. As presented in Figure 5, raw SBA-15, MCM-41 and FS showed very low contact angle values (12.6◦, 11.5◦, 16.8◦, respectively). The water droplet spread promptly all over solid particulate surfaces resulting in 0◦ contact angle within 2 sec. This result can be explained by the strong hydrophilicity of silica surfaces due to their abundant hydroxyl surface groups that are able to form hydrogen bonds with water molecules. Another reason is capillary action (wicking) of water through silica substrate due to the presence of nano-sized pores [53]. To determine the wettability of the drug, KAZ3 was sprayed using ethanol or acetone and the contact angle was measured. In both cases, the contact angle was high (> 90◦), highlighting the high hydrophobicity of the drug irrespective of the solvent used. To further evaluate the presence of drug on or within particles, the contact angle of all formulations was measured. As shown in Figure 5, the contact angle of all solvent impregnated formulations is similar to pristine mesoporous silica, indicating that mesoporous silica preserves its hydrophilicity, since the abundant free hydroxyl groups do not decrease with this technique. Also, contact angle values might be low because of the crystalline\semi crystalline nature of the surface adsorbed active [52]. In contrast, the contact angle of atomized formulations was prominently higher than raw silica and solvent impregnated formulations with values ranging from 90^{o} to 103^{o}. This is attributed to the decrease of the free hydroxyl groups, possibly due to the interactions developed with the drug molecules, therefore decreasing hydrogen bonding with water. In addition, the wicking effect is also reduced as pores are partially blocked with drug. However, a reduction in contact angle over time was observed and varied depending on atomized formulations.

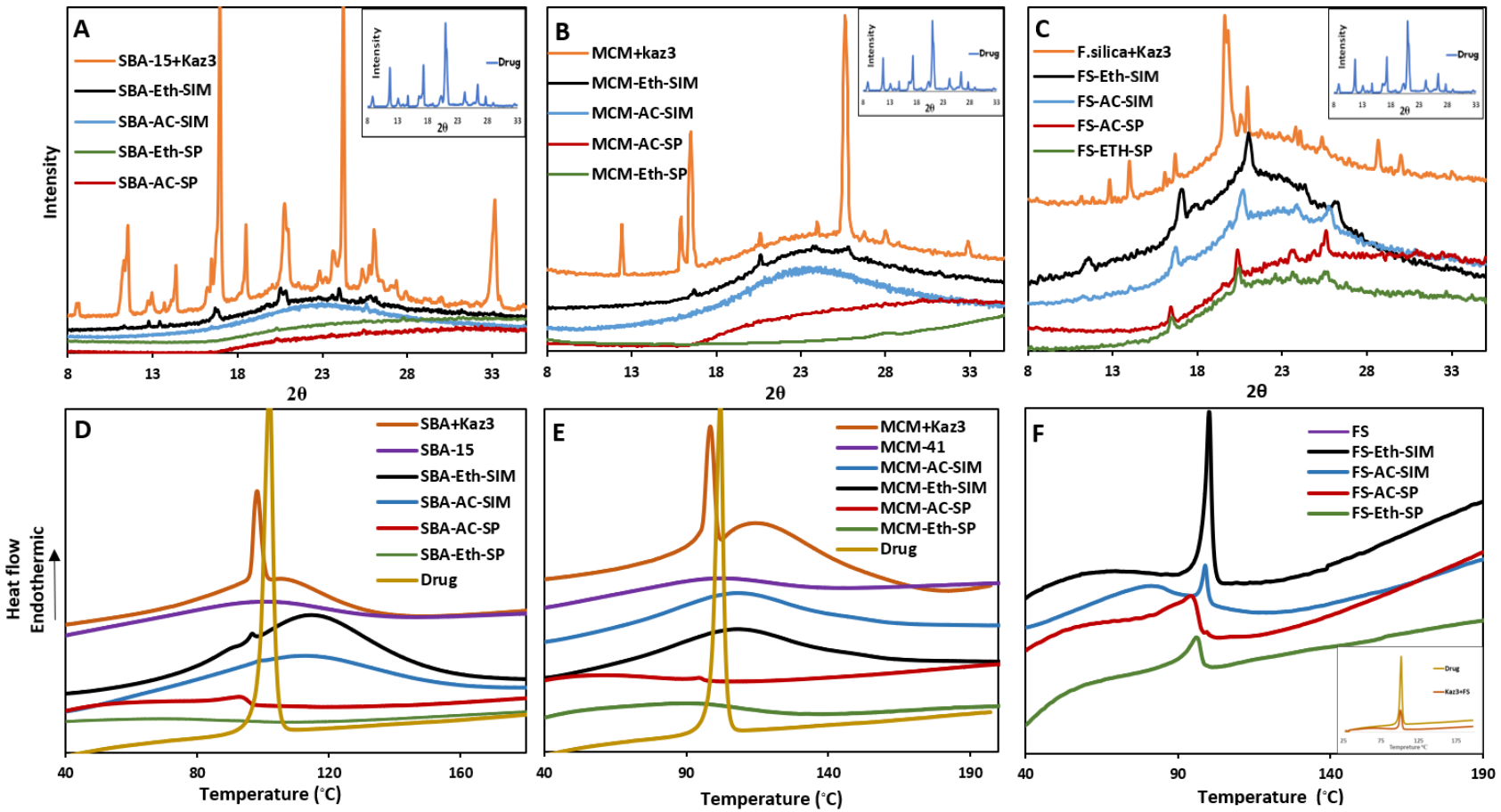

Figure 4. A., B., C. XRD patterns and **D., E., F.** DSC thermograms of pristine silica materials and drug loaded formulations**.** SBA: SBA-15, MCM: MCM-41, FS: fumed silica, Eth: Ethanol, AC: acetone, SIM: solvent impregnation method and SP: electrospraying method.

For example, the contact angle of SBA-Eth-SP was 90° at 0 seconds and attained its lowest value (4.3°) within 10 seconds. This reflects that drug dissolution occurs once water molecules penetrate through the pores. The respective contact angle values for SBA-AC-SP was 103° and reached 0° after 1 h. This is attributed to the higher loading efficiency of SBA-AC-SP than SBA-Eth-SP. Similar findings were obtained with MCM-41 based atomized formulations. With regard to non-porous atomized formulations (FS-Eth-SP and FS-AC-SP), values of 104° and 95° were obtained at 0 sec, respectively. However, their contact angle took a longer time to decrease than atomized mesoporous formulations (Figure 5), due to the lower dissolution rate of the adsorbed drug in formulations.

In particular, contact angle studies revealed that the ethanol sprayed formulations were more hydrophilic compared to their acetone congeners. It is anticipated by extrapolation to the *in vivo* situation that the clearance of hydrophobic formulations would be slower; the latter, however, provides drug released amounts over extended periods of time that would be beneficial to the cellular absorption process. Complementary, it should be emphasized that hydrophobicity is a crucial factor contributing to cellular membrane permeability, since molecules are facilitated to move through the lipophilic structures. To this end, the bioaccumulation of the electrosprayed formulations is expected to be positively influenced by their hydrophobic nature, thus leading to increased permeable drug concentrations and enhanced bioavailability, especially for poorly soluble drugs.

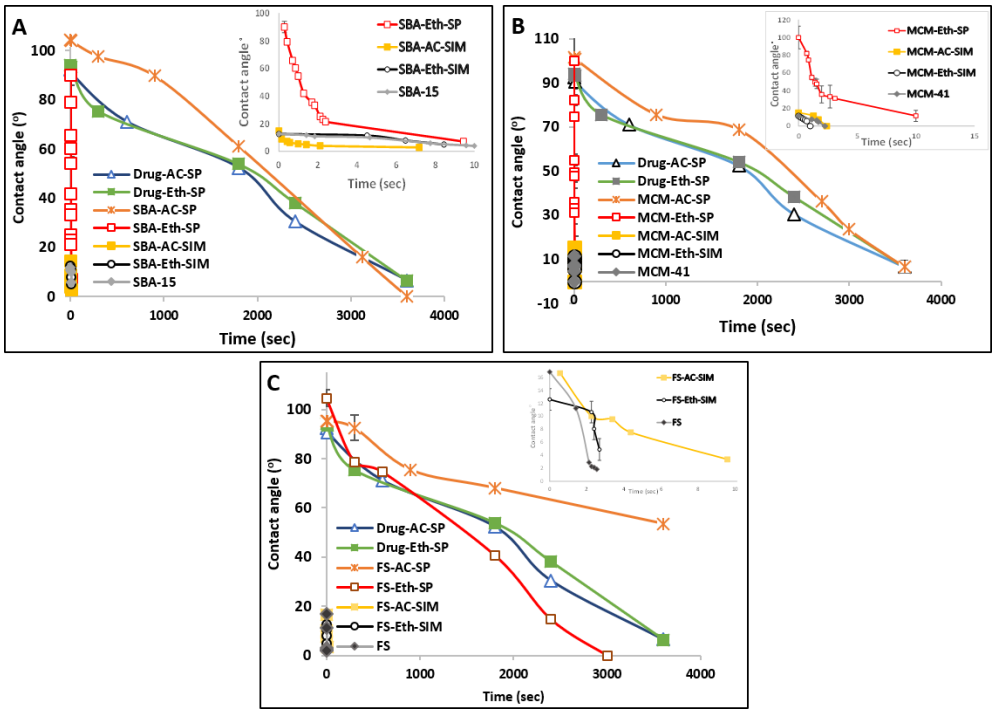

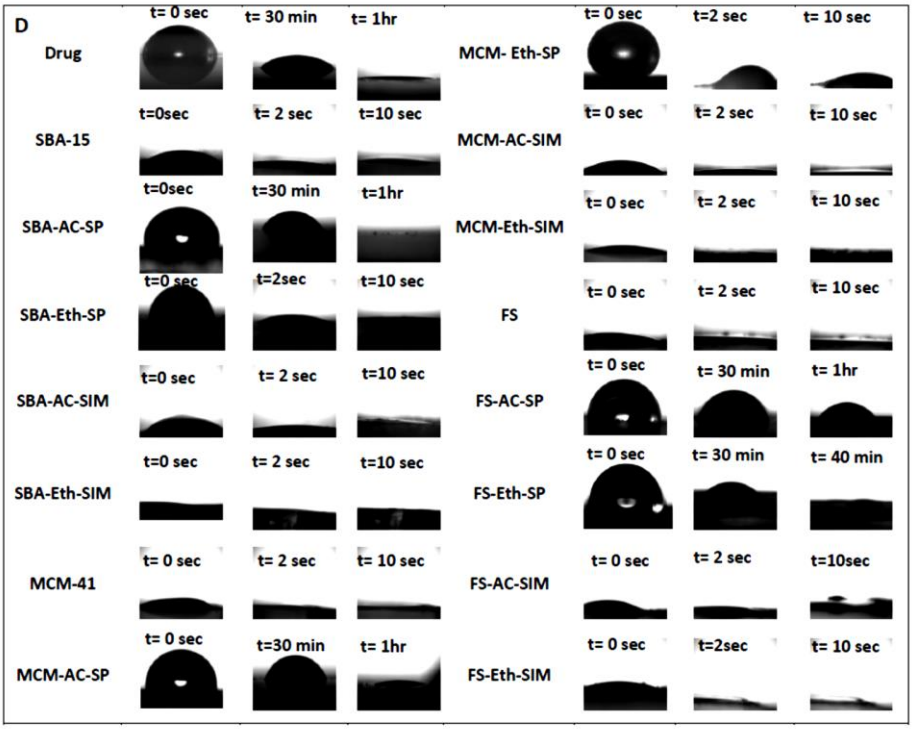

Figure 5. Plots of θ° values versus time for **A.** SBA-15, **B**. MCM-41 and **C**. FS before and after drug loading and **D**. digital images captured at different time intervals. Where

630 SBA: SBA-15, MCM: MCM-41, FS: fumed silica, Eth: Ethanol, AC: acetone, SIM:
631 solvent impregnation method and SP: electrospraying method.
632
633 3.9. *In vitro* release studies
634 *In vitro* release profiles of KAZ3 from all formulations are presented in Figure 6. Drug
635 release from the loaded mesoporous silica particles showed a bi-phasic pattern with an
636 initial burst release followed by a subsequent plateau. The dissolution rate of the drug
637 from the atomized drug loaded mesoporous silica particles was prominently higher than
638 from the formulations prepared using solvent impregnation (t-test, $p<0.05$), reaching a
639 total of 19 % to 37.5 % drug release within 1 hr. On the other hand, solvent impregnated
640 formulations only achieved a total of 4 % to 17 % drug release at the same time course.
641 After 24 h electrosprayed formulations released between 41 % to 72 % of their drug
642 content, while formulations loaded using the solvent impregnation method released
643 between 10 % to 38 % of their total drug content. Conversely, pure crystalline drug and
644 formulations based on FS achieved a total of 2 % and 6 % to 19 % of drug release,
645 respectively after 24 h. This indicates that incorporation of drug within mesopores has
646 a pronounced effect on solubility enhancement.
647 Drug dissolution showed a 35-fold enhancement using EHDA compared to the raw
648 crystalline drug. Solvent impregnated formulations with high crystallinity (33.2 % -
649 79.9 %) exhibited a lower dissolution rate when compared to electrosprayed
650 formulations. This significant enhancement in drug's dissolution properties by
651 electrospraying is not only attributed to KAZ3 amorphization, but also to the lower
652 particle size of the electrosprayed formulations. By decreasing silica particle size, the
653 diffusion distance of the drug is reduced, thus improving its release rate [8]. In contrast,

the presence of solvent impregnated silica particles yielded aggregates which partially block pores, increasing the drug diffusion distance to the dissolution media.

Although larger pores result to greater dissolution rates, no significant differences were observed between the dissolution profiles of SBA-15 and MCM-41-based formulations. This observation may be a result of the lower particle size of atomized MCM-41 than atomized SBA-15, which may have compensated for the reduced pore size [8]. However, a significant difference was observed between the dissolution rates of mesoporous silica-based formulations and non-porous particulates. Nonporous formulations released between 6.6 % to 18.7 % of their drug content by the end of the experiment. This demonstrates that incorporation of drug in nano-sized pores clearly improves dissolution more than interactions with surface silanol groups.

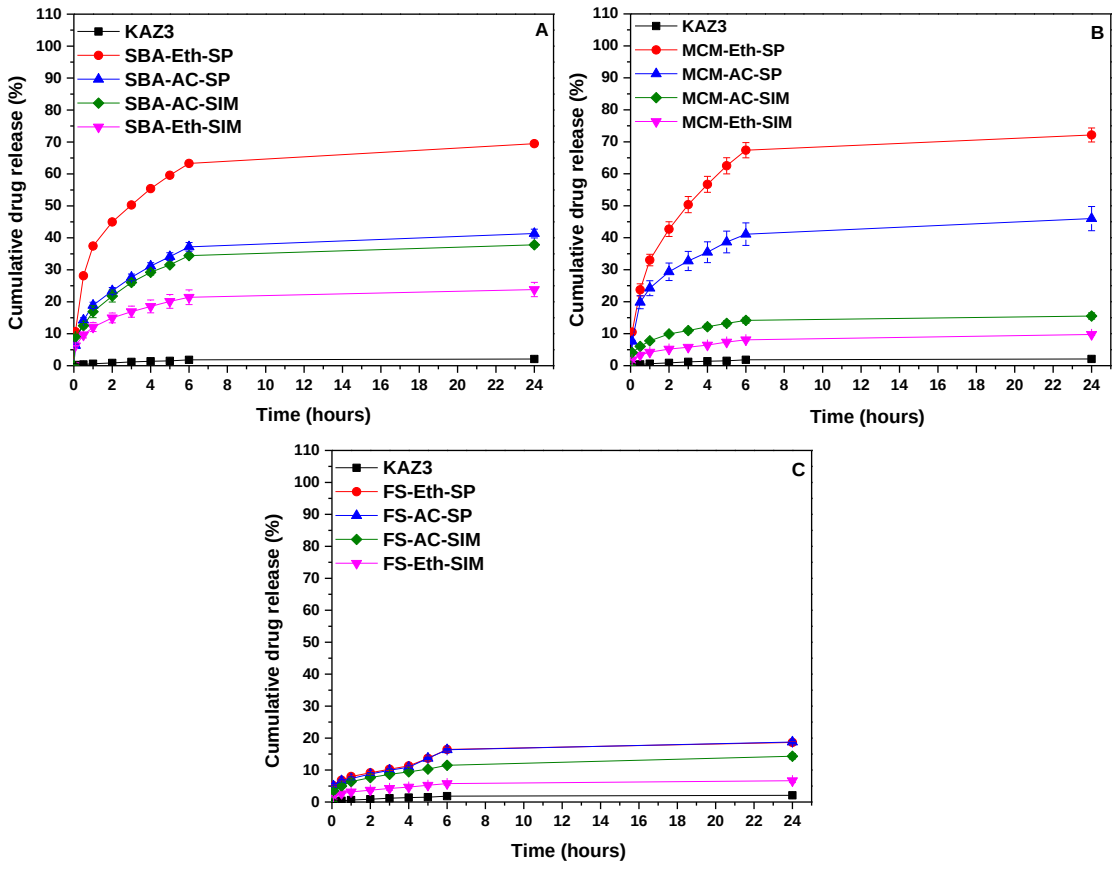

Figure 6. *In vitro* release profiles of pure KAZ3 and KAZ3 loaded silica particles **A.** SBA-15, **B.** MCM-41 and **C**. FS using different solvents and loading methods (n=3). SBA: SBA-15, MCM: MCM-41, FS: fumed silica, Eth: Ethanol, AC: acetone, SIM: solvent impregnation method and SP: electrospraying method.

3.10. Release kinetics

The diffusion release kinetics in porous carriers is well illustrated using Higuchi and Korsmeyer-Peppas kinetic models [54-60]. The data obtained from the *in vitro* release studies were fitted to Higuchi [61] and Korsmeyer-Peppas [62] kinetic models (SM, Figure S9). A curve fitting analysis was performed to determine the release kinetic parameters (SM, Table S6).

Applying the Higuchi model (SM, Figure S9 A, B & C) all formulations demonstrated two-step release kinetics with high R^2 values for both stages. The R^2 values were ≥ 0.96 for the mesoporous silica-based formulations and ≤ 0.96 for the non-porous formulations. This high correlation coefficient suggests that the mechanism of release for KAZ3 through these systems is Fickian diffusion. However, the occurrence of a two-step release mechanism is possibly due to alterations to silica's dissolution rate over time [55]. Similar two-step release kinetics for mesoporous materials for the Higuchi model have been previously reported in the literature [55-58]. The greatest K_H value was attained for the electrosprayed mesoporous silica-based formulations indicating a better drug release compared to other systems. However, the release rate constant varied, depending on the silica type and the solvent used for the atomization process (SM, Table S6).

The first 60 % of the *in vitro* release data were fitted to Korsmeyer-Peppas as shown in SM Figure S9 D, E & F. The obtained kinetic parameters (R^2 and n: diffusion or release

exponent that characterizes the release mechanism of the drug) are presented in SM, Table S6. The plots of all formulations showed a linear fit to Korsmeyer-Peppas model (R^2: 0.91 - 0.99). The n values of ethanol atomized formulations (MCM-Eth-SP and SBA-Eth-SP) were approximately 0.43, indicative of Fickian diffusion mechanism. However, the n values of the other formulations ranged between 0.25 to 0.35. This deviation could be attributed to the wide particle size distribution [62], resulting to fluctuations in diffusion times. The broader the size distribution [represented by span value (SM, Table S3)] the lower the n value. It is noteworthy that some studies have referred to the instance $n < 0.43$ as quasi-Fickian diffusion [63,64].

3.11 *Ex vivo* intestinal permeability studies

Cumulative permeation profiles of KAZ3 dispersion and KAZ3 after loading in different silica substrates (SBA-15, MCM-41, FS) utilizing different loading techniques (electrospraying and solvent impregnation) were determined by using the non-everted intestinal sac method. Results indicated that KAZ3 in suspension form demonstrated poor permeability across the intestinal membrane, owing to its low solubility in the mucosal compartment. Similar permeability profiles were obtained for all formulations prepared *via* the solvent impregnation method, as well (Figure 7). On the contrary, a substantial permeation enhancement of the drug was observed for all formulations prepared *via* the electrospraying method. Such significant enhancement in KAZ3 could be related to the drug solubilizing effect of the electrospraying method, as already demonstrated in the *in vitro* release studies. The increment in the permeation enhancing effect followed the order: MCM-41 > SBA-15 > FS, being in close agreement with the *in vitro* KAZ3 release profiles.

All electrosprayed mesoporous formulations reported statistically significant higher J_{ss} and P_{app} values ($p < 0.05$), compared to both KAZ3 suspension and formulations prepared *via* the solvent impregnation method, as shown in Table 2. MCM-Eth-SP formulation showed the highest P_{app} achieving a 9.45-fold increase relative to the drug suspension. Similarly to the present study, it has been previously demonstrated that the adoption of various formulation approaches that result to improved drug solubility and dissolution rates can further contribute to improved intestinal permeability over plain drug suspensions [65,66].

Table 2. Apparent permeability (P_{app}) and steady state flux **(**J_{ss}**)** values of KAZ3 from different formulations using the non-everted intestinal sac method (n=3-5).

Sample	J_{ss} (ng/min/cm^2)	$P_{app} \cdot 10^{-7}$ (cm/s)	Enhancement Ratio
KAZ3 suspension	0.22 ± 0.02	8.88 ± 0.8	1
SBA-Eth-SIM	0.21 ± 0.07	8.32 ± 2.8	0.9
SBA-Eth-SP	0.63 ± 0.03	25.30 ± 1.2	2.8
MCM-Eth-SIM	0.09 ± 0.01	3.60 ± 0.4	0.4
MCM-Eth-SP	2.10 ± 0.02	84.0 ± 0.8	9.45
FS-Eth-SIM	0.31 ± 0.01	12.5 ± 0.40	1.4
FS-Eth-SP	0.83 ± 0.01	33.2 ± 0.39	3.7

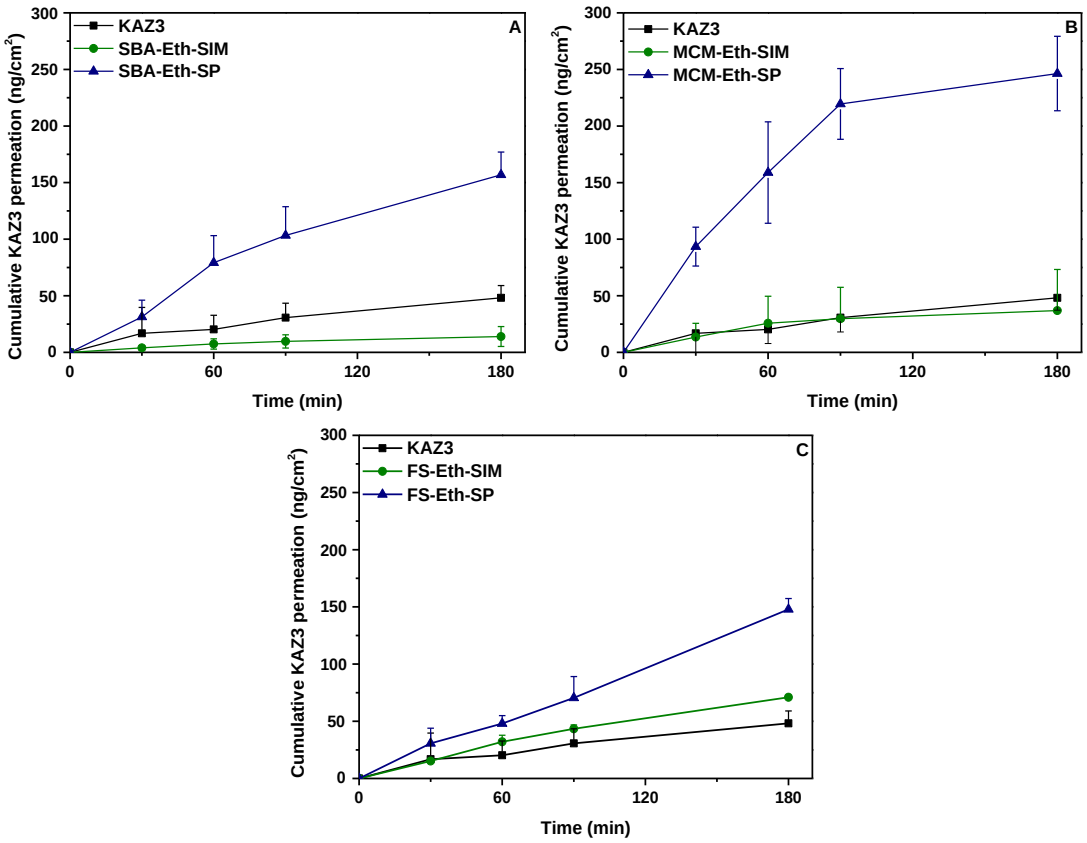

Figure 7. *Ex vivo* permeation profiles of plain drug and drug loaded in **A**. SBA-15, **B**. MCM-41 and **C.** FS particles using the non-everted sac method in Krebs-Ringer solution at 37 ºC (n=3-5). SBA: SBA-15, MCM: MCM-41, FS: fumed silica, Eth: Ethanol, AC: acetone, SIM: solvent impregnation method and SP: electrospraying method.

3.12 Cytocompatibility studies

The IC_{50} of KAZ3 was calculated to be 6.905 μM (Figure 8A). The suitability of ordered mesoporous silica MCM and SBA for oral drug formulations has been previously thoroughly assessed on Caco-2 cells [67]. A moderate effect on cell viability was observed for most concentrations and incubation times evaluated, while particle size and shape were also found to partly contribute to cytotoxicity. In the present study, the cytotoxic effect of the drug loaded MCM, SBA and FS particles was evaluated at the

concentrations of 0.1 mg/mL and 1 mg/mL on Caco-2 cells after 4 h, 24 h and 48 h of cell exposure to the dispersions (Figure 8 B, C & D).

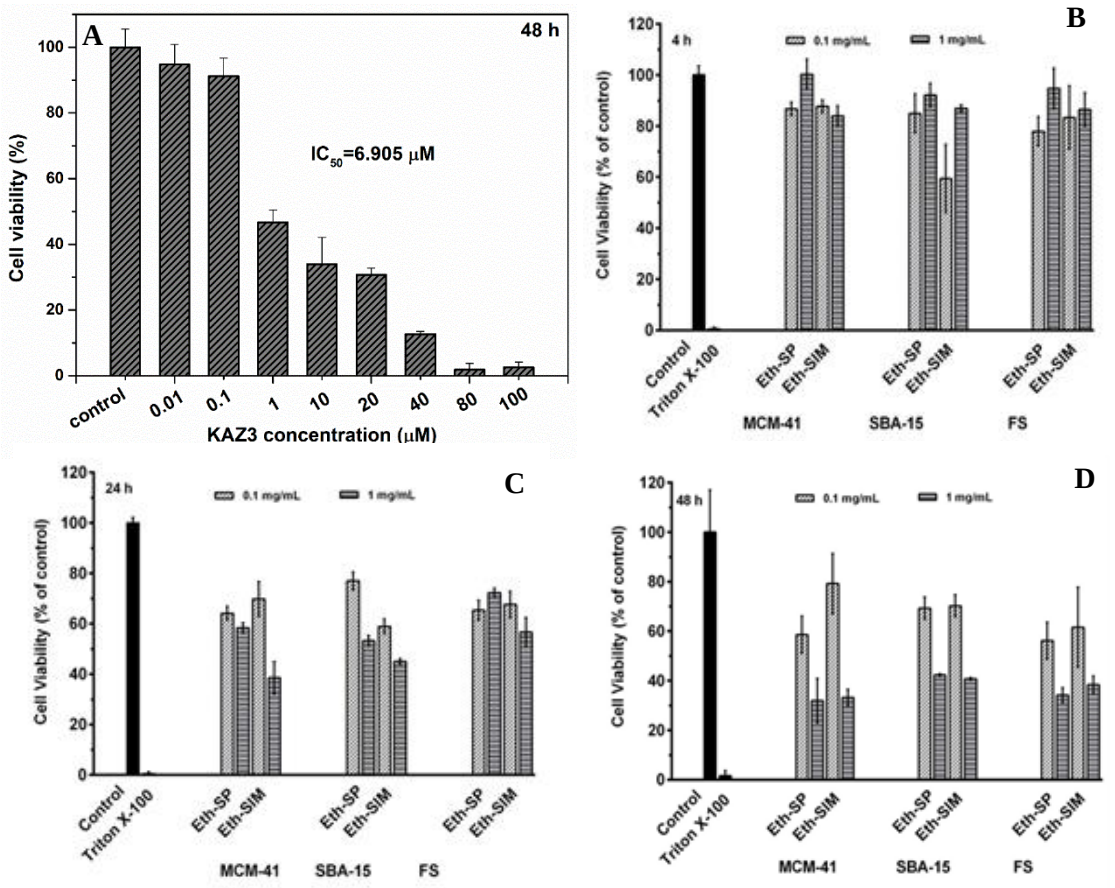

Figure 8. **A**. Assessment of cell viability of Caco-2 cells exposed to KAZ3 (n=3). The cellular viability of Caco-2 cell cultures without treatment (negative control), after treatment with 1 % Triton X-100 (positive control) and after incubation with 0.1 mg/mL and 1 mg/mL of KAZ3-loaded MCM-41, SBA-15 and FS materials, for **B.** 4 h, **C**. 24 h and **D.** 48h was assessed by MTT assay (n=3). Eth: Ethanol, AC: acetone, SIM: solvent impregnation method and SP: electrospraying method.

No significant effect on cell viability (> 80 %) was observed after 4 h of incubation for most formulations at both concentrations tested. On the contrary, a higher cytotoxic effect was induced after 24 h and 48 h of cell exposure to the tested formulations, with

796 the effect being more pronounced (< 60 %) at the concentration of 1 mg/mL. The
797 cellular morphology of Caco-2 cells exposed to KAZ3 for either 24 h or 48 h was altered
798 at concentrations ≥ 1 μM (SM, Figure S10), a fact coinciding with the capacity of this
799 agent to affect cell proliferation of Caco-2 cells (Figure 8 A). The capacity of KAZ3-
800 loaded MCM, SBA and FS formulations to cause cytotoxicity and affect the
801 proliferation of Caco-2 cells exposed for 48 h at 0.1 mg/mL and 1 mg/mL is also
802 indicated by assessing the cellular morphology (SM, Figure S11). The latter, coincides
803 with the effect of these formulations to decrease the viability of Caco-2 cell cultures, as
804 seen in Figure 8 D.
805
806 **Conclusions**
807 To obtain a comprehensive overview of the potentiality of electrospraying as a
808 successful strategy to improve the solubility of poorly soluble compounds an in-depth
809 study was conducted utilizing mesoporous (SBA-15, MCM-41) and non-porous (fumed
810 silica) silica materials as the drug carriers of a sparingly water-soluble anticancer agent;
811 a novel chalcone (KAZ3). Two different approaches were utilized to encapsulate the
812 anticancer agent to the particles namely; electrospraying and solvent impregnation
813 method whereas an array of analytical methods was employed to characterize the empty
814 and drug loaded carriers. The electrosprayed mesoporous formulations demonstrated
815 uniform particle size, high drug loading efficiencies with the drug encapsulated in an
816 amorphous state, while at the same time a significant enhancement in drug dissolution
817 up to 30-fold and drug intestinal permeability up to 9.45-fold was observed, compared
818 to the pure crystalline drug, mainly due to drug amorphization on the silica carriers.
819 Contact angle goniometry studies offered insights on the wettability properties of the
820 mesoporous carriers further corroborating the *in vitro* and *ex vivo* data, whereas

molecular dynamics offered a unique insight into the interactions between the drug and the framework and could prove to be a valuable tool in screening drug-mesoporous combinations for further experimental investigation. Importantly, the mesoporous loaded material exhibited moderate toxicity as observed by the kinetics of cell proliferation and the assessment of cell viability in Caco-2 cell cultures. Overall, the findings of the present study underlie the potential of electrosprayed silica hybrids for further research for *in vivo* biomedical applications.

Acknowledgement

The authors would like to gratefully acknowledge the Egyptian Culture Centre and the Educational Bureau in London for funding the research. The authors would also like to thank the EPSRC (EPSRC EHDA Network) for their support.

Declaration of interest

None

References

[1] M. Pilatova, L. Varinska, P. Perjesi, M. Sarissky, L. Mirossay, P. Solar, A. Ostro, J. Mojzis, In vitro antiproliferative and antiangiogenic effects of synthetic chalcone analogues, Toxicol in Vitro. 24 (2010) 1347-1355.

[2] M. Shahbazi, B. Herranz, H.A. Santos, Nanostructured porous Si-based nanoparticles for targeted drug delivery, Biomatter. 2 (2012) 296-312.

[3] S. Won, C. Liu, L. Tsao, J. Weng, H. Ko, J. Wang, C. Lin, Synthetic chalcones as potential anti-inflammatory and cancer chemopreventive agents, Eur. J. Med. Chem. 40 (2005) 103-112.

[4] M. Das, K. Manna, Chalcone scaffold in anticancer armamentarium: a molecular insight, Journal of toxicology. 2016 (2016).

[5] R. De Vincenzo, C. Ferlini, M. Distefano, C. Gaggini, A. Riva, E. Bombardelli, P. Morazzoni, P. Valenti, F. Belluti, F.O. Ranelletti, In vitro evaluation of newly developed chalcone analogues in human cancer cells, Cancer Chemother. Pharmacol. 46 (2000) 305-312.

[6] C. Echeverria, J.F. Santibañez, O. Donoso-Tauda, C.A. Escobar, R. Ramirez-Tagle, Structural antitumoral activity relationships of synthetic chalcones, Int. J. Mol. Sci. 10 (2009) 221-231.

[7] M.N. Gomes, E.N. Muratov, M. Pereira, J.C. Peixoto, L.P. Rosseto, P.V. Cravo, C.H. Andrade, B.J. Neves, Chalcone Derivatives: Promising Starting Points for Drug Design, Molecules. 22 (2017) 1210.

[8] S. Hong, S. Shen, D.C.T. Tan, W.K. Ng, X. Liu, L.S. Chia, A.W. Irwan, R. Tan, S.A. Nowak, K. Marsh, High drug load, stable, manufacturable and bioavailable fenofibrate formulations in mesoporous silica: a comparison of spray drying versus solvent impregnation methods, Drug Deliv. 23 (2016) 316-327.

871 [9] J. Xie, J. Jiang, P. Davoodi, M.P. Srinivasan, C. Wang, Electrohydrodynamic
872 atomization: A two-decade effort to produce and process micro-/nanoparticulate
873 materials, Chem. Eng. Sci. 125 (2015) 32-57.
874 [10] Y. Zhang, J. Wang, X. Bai, T. Jiang, Q. Zhang, S. Wang, Mesoporous silica
875 nanoparticles for increasing the oral bioavailability and permeation of poorly water
876 soluble drugs, Mol. Pharm. 9 (2012) 505-513.
877 [11] C. Leuner, J. Dressman, Improving drug solubility for oral delivery using solid
878 dispersions, Eur. J. Pharm. Biopharm. 50 (2000) 47-60.
879 [12] R. Mellaerts, J.A. Jammaer, M. Van Speybroeck, H. Chen, J.V. Humbeeck, P.
880 Augustijns, G. Van den Mooter, J.A. Martens, Physical state of poorly water soluble
881 therapeutic molecules loaded into SBA-15 ordered mesoporous silica carriers: a case
882 study with itraconazole and ibuprofen, Langmuir. 24 (2008) 8651-8659.
883 [13] T. Vasconcelos, B. Sarmento, P. Costa, Solid dispersions as strategy to improve
884 oral bioavailability of poor water-soluble drugs, Drug Discov. Today. 12 (2007) 1068-
885 1075.
886 [14] A. Fahr, X. Liu, Drug delivery strategies for poorly water-soluble drugs, Expert
887 opinion on drug delivery. 4 (2007) 403-416.
888 [15] E. Merisko-Liversidge, G.G. Liversidge, Nanosizing for oral and parenteral drug
889 delivery: A perspective on formulating poorly-water soluble compounds using wet
890 media milling technology, Adv. Drug Deliv. Rev. 63 (2011) 427-440.
891 [16] A. Figueiras, R.A. Carvalho, L. Ribeiro, J.J. Torres-Labandeira, F.J.B. Veiga,
892 Solid-state characterization and dissolution profiles of the inclusion complexes of
893 omeprazole with native and chemically modified β-cyclodextrin, Eur. J. Pharm.
894 Biopharm. 67 (2007) 531-539.

[17] A. Paudel, Z.A. Worku, J. Meeus, S. Guns, G. Van den Mooter, Manufacturing of solid dispersions of poorly water-soluble drugs by spray drying: Formulation and process considerations, Int. J. Pharm. 453 (2013) 253-284.

[18] S. Zhang, K. Kawakami, M. Yamamoto, Y. Masaoka, M. Kataoka, S. Yamashita, S. Sakuma, Coaxial electrospray formulations for improving oral absorption of a poorly water-soluble drug, Mol. Pharm. 8 (2011) 807-813.

[19] V. Ambrogi, L. Perioli, F. Marmottini, S. Giovagnoli, M. Esposito, C. Rossi, Improvement of dissolution rate of piroxicam by inclusion into MCM-41 mesoporous silicate, Eur. J. Pharm. Sci. 32 (2007) 216-222.

[20] T. Heikkilä, J. Salonen, J. Tuura, N. Kumar, T. Salmi, D.Y. Murzin, M. Hamdy, G. Mul, L. Laitinen, A. Kaukonen, Evaluation of mesoporous TCPSi, MCM-41, SBA-15, and TUD-1 materials as API carriers for oral drug delivery, Drug Deliv. 14 (2007) 337-347.

[21] R. Mellaerts, R. Mols, J.A.G. Jammaer, C.A. Aerts, P. Annaert, J. Van Humbeeck, G. Van den Mooter, P. Augustijns, J.A. Martens, Increasing the oral bioavailability of the poorly water-soluble drug itraconazole with ordered mesoporous silica, Eur J Pharm Biopharm. 69 (2008) 223-230.

[22] M.J.K. Thomas, I. Slipper, A. Walunj, A. Jain, M.E. Favretto, P. Kallinteri, D. Douroumis, Inclusion of poorly soluble drugs in highly ordered mesoporous silica nanoparticles, Int. J. Pharm. 387 (2010) 272-277.

[23] R.J. Ahern, J.P. Hanrahan, J.M. Tobin, K.B. Ryan, A.M. Crean, Comparison of fenofibrate–mesoporous silica drug-loading processes for enhanced drug delivery, Eur. J. Pharm. Sci. 50 (2013) 400-409.

[24] P. Gao, Amorphous pharmaceutical solids: characterization, stabilization, and development of marketable formulations of poorly soluble drugs with improved oral absorption, Mol. Pharm. 5 (2008) 903-904.

[25] J.M. Rosenholm, C. Sahlgren, M. Lindén, Towards multifunctional, targeted drug delivery systems using mesoporous silica nanoparticles–opportunities & challenges, Nanoscale. 2 (2010) 1870-1883.

[26] C. Lee, S. Cheng, I. Huang, J.S. Souris, C. Yang, C. Mou, L. Lo, Intracellular pH-responsive mesoporous silica nanoparticles for the controlled release of anticancer chemotherapeutics, Angewandte Chemie. 122 (2010) 8390-8395.

[27] S. Song, K. Hidajat, S. Kawi, Functionalized SBA-15 materials as carriers for controlled drug delivery: influence of surface properties on matrix-drug interactions, Langmuir. 21 (2005) 9568-9575.

[28] P. Horcajada, A. Ramila, J. Perez-Pariente, M. Vallet-Regı, Influence of pore size of MCM-41 matrices on drug delivery rate, Microporous Mesoporous Mater. 68 (2004) 105-109.

[29] E. Sayed, R. Haj-Ahmad, K. Ruparelia, M. Arshad, M. Chang, Z. Ahmad, Porous Inorganic Drug Delivery Systems—a Review, AAPS PharmSciTech. 18 (2017) 1507-1525.

[30] R.J. Ahern, A.M. Crean, K.B. Ryan, The influence of supercritical carbon dioxide (SC-CO2) processing conditions on drug loading and physicochemical properties, Int. J. Pharm. 439 (2012) 92-99.

[31] J. Lu, M. Liong, J.I. Zink, F. Tamanoi, Mesoporous silica nanoparticles as a delivery system for hydrophobic anticancer drugs, Small. 3 (2007) 1341-1346.

[32] J. Lu, M. Liong, S. Sherman, T. Xia, M. Kovochich, A.E. Nel, J.I. Zink, F. Tamanoi, Mesoporous silica nanoparticles for cancer therapy: energy-dependent

943 cellular uptake and delivery of paclitaxel to cancer cells, Nanobiotechnology. 3 (2007)
944 89-95.
945 [33] L.J. Waters, T. Hussain, G. Parkes, J.P. Hanrahan, J.M. Tobin, Inclusion of
946 fenofibrate in a series of mesoporous silicas using microwave irradiation, Eur J Pharm
947 Biopharm. 85 (2013) 936-941.
948 [34] M. Zamani, M.P. Prabhakaran, S. Ramakrishna, Advances in drug delivery via
949 electrospun and electrosprayed nanomaterials, Int J Nanomedicine. 8 (2013) 2997-
950 3017.
951 [35] M. Rasekh, A. Smith, M. S Arshad, O. Gunduz, M Van der Merwe, S, G. Smith,
952 Z. Ahmad, Electrohydrodynamic preparation of nanomedicines, Curr. Top. Med.
953 Chem. 15 (2015) 2316-2327.
954 [36] H. Lin, C. Tang, C. Lin, Detailed structural characterizations of sba-15 and mcm-
955 41 mesoporous silicas on a high-resolution transmission electron microscope, J. Chin.
956 Chem. Soc. 49 (2002) 981-988.
957 [37] L. Giraldo, B. López, L. Pérez, S. Urrego, L. Sierra, M. Mesa, Mesoporous silica
958 applications, Macromol. Symp. 258 (2007) 129-141.
959 [38] D.N. Dhar, The Chemistry of Chalcones and Related Compounds, John Wiley &
960 Sons, 1981.
961 [39] S. Dessault, BIOVIA Materials Studio, Release 2017. San Diego (2017).
962 [40] D. Zhao, J. Feng, Q. Huo, N. Melosh, G.H. Fredrickson, B.F. Chmelka, G.D.
963 Stucky, Triblock copolymer syntheses of mesoporous silica with periodic 50 to 300
964 angstrom pores, Science. 279 (1998) 548-552.
965 [41] K. Dimos, P. Stathi, M.A. Karakassides, Y. Deligiannakis, Synthesis and
966 characterization of hybrid MCM-41 materials for heavy metal adsorption, Microporous
967 and Mesoporous Materials. 126 (2009) 65-71.

968 [42] N. Miriyala, D. Ouyang, Y. Perrie, D. Lowry, D.J. Kirby, Activated carbon as a
969 carrier for amorphous drug delivery: Effect of drug characteristics and carrier
970 wettability, Eur. J. Pharm. Biopharm. 115 (2017) 197-205.
971 [43] C. Karavasili, M. Spanakis, D. Papagiannopoulou, I.S. Vizirianakis, D.G.
972 Fatouros, S. Koutsopoulos, Bioactive Self-Assembling Lipid-Like Peptides as
973 Permeation Enhancers for Oral Drug Delivery, J. Pharm. Sci. 104 (2015) 2304-2311.
974 [44] T. Mosmann, Rapid colorimetric assay for cellular growth and survival:
975 Application to proliferation and cytotoxicity assays, J. Immunol. Methods. 65 (1983)
976 55-63.
977 [45] C. Karavasili, E.P. Amanatiadou, E. Kontogiannidou, G.K. Eleftheriadis, N.
978 Bouropoulos, E. Pavlidou, I. Kontopoulou, I.S. Vizirianakis, D.G. Fatouros,
979 Comparison of different zeolite framework types as carriers for the oral delivery of the
980 poorly soluble drug indomethacin, Int. J. Pharm. 528 (2017) 76-87.
981 [46] D. Rath, S. Rana, K. Parida, Organic amine-functionalized silica-based
982 mesoporous materials: an update of syntheses and catalytic applications, RSC
983 Advances. 4 (2014) 57111-57124.
984 [47] P. Mehta, A.A. Al-Kinani, R. Haj-Ahmad, M.S. Arshad, M. Chang, R.G. Alany,
985 Z. Ahmad, Electrically atomised formulations of timolol maleate for direct and on-
986 demand ocular lens coatings, Eur. J. Pharm. Biopharm. 119 (2017) 170-184.
987 [48] K.K. Qian, R.H. Bogner, Application of Mesoporous Silicon Dioxide and Silicate
988 in Oral Amorphous Drug Delivery Systems, J. Pharm. Sci. 101 (2012) 444-463.
989 [49] S. Kumar, M. Gradzielski, S. Mehta, The critical role of surfactants towards CdS
990 nanoparticles: synthesis, stability, optical and PL emission properties, RSC Advances.
991 3 (2013) 2662-2676.

992 [50] S. Shen, W.K. Ng, L. Chia, J. Hu, R.B.H. Tan, Physical state and dissolution of
993 ibuprofen formulated by co-spray drying with mesoporous silica: Effect of pore and
994 particle size, Int. J. Pharm. 410 (2011) 188-195.
995 [51] Y. Zhang, Z. Zhi, T. Jiang, J. Zhang, Z. Wang, S. Wang, Spherical mesoporous
996 silica nanoparticles for loading and release of the poorly water-soluble drug telmisartan,
997 J. Control. Release. 145 (2010) 257-263.
998 [52] C.F. Fan, T. Cağin, Wetting of crystalline polymer surfaces: A molecular dynamics
999 simulation, J. Chem. Phys. 103 (1995) 9053-9061.
1000 [53] C.S. Thompson, R.A. Fleming, M. Zou, Transparent self-cleaning and antifogging
1001 silica nanoparticle films, Sol. Energy Mater Sol. Cells. 115 (2013) 108-113.
1002 [54] G. Maria, D. Berger, S. Nastase, I. Luta, Kinetic studies on the irinotecan release
1003 based on structural properties of functionalized mesoporous-silica supports,
1004 Microporous and Mesoporous Materials. 149 (2012) 25-35.
1005 [55] J. Andersson, J. Rosenholm, S. Areva, M. Lindén, Influences of material
1006 characteristics on ibuprofen drug loading and release profiles from ordered micro-and
1007 mesoporous silica matrices, Chem. Mater. 16 (2004) 4160-4167.
1008 [56] A.L. Doadrio, E.M.B. Sousa, J.C. Doadrio, J. Pérez Pariente, I. Izquierdo-Barba,
1009 M. Vallet-Regí, Mesoporous SBA-15 HPLC evaluation for controlled gentamicin drug
1010 delivery, J. Controlled Release. 97 (2004) 125-132.
1011 [57] J. Andersson, S. Areva, B. Spliethoff, M. Lindén, Sol–gel synthesis of a
1012 multifunctional, hierarchically porous silica/apatite composite, Biomaterials. 26 (2005)
1013 6827-6835.
1014 [58] M. Ghasemnejad, E. Ahmadi, Z. Mohamadnia, A. Doustgani, S. Hashemikia,
1015 Functionalized silica nanoparticles as a carrier for Betamethasone Sodium Phosphate:

Drug release study and statistical optimization of drug loading by response surface method, Mater Sci Eng C. 56 (2015) 223-232.

[59] P. Nadrah, U. Maver, A. Jemec, T. Tišler, M. Bele, G. Dražić, M. Benčina, A. Pintar, O. Planinšek, M. Gaberšček, Hindered disulfide bonds to regulate release rate of model drug from mesoporous silica, ACS Appl. Mater. Interfaces. 5 (2013) 3908-3915.

[60] S. Wang, Ordered mesoporous materials for drug delivery, Microporous Mesoporous Mater. 117 (2009) 1-9.

[61] S. Dash, P.N. Murthy, L. Nath, P. Chowdhury, Kinetic modelling on drug release from controlled drug delivery systems, Acta Pol. Pharm. 67 (2010) 217-223.

[62] P.L. Ritger, N.A. Peppas, A simple equation for description of solute release I. Fickian and non-fickian release from non-swellable devices in the form of slabs, spheres, cylinders or discs, J. Control. Release. 5 (1987) 23-36.

[63] S.N. Park, M.H. Lee, S.J. Kim, E.R. Yu, Preparation of quercetin and rutin-loaded ceramide liposomes and drug-releasing effect in liposome-in-hydrogel complex system, Biochem. Biophys. Res. Commun. 435 (2013) 361-366.

[64] P.P. Nerkar, S. Gattani, In vivo, in vitro evaluation of linseed mucilage based buccal mucoadhesive microspheres of venlafaxine, Drug Deliv. 18 (2011) 111-121.

[65] M.S. Freag, Y.S.R. Elnaggar, O.Y. Abdallah, Development of novel polymer-stabilized diosmin nanosuspensions: In vitro appraisal and ex vivo permeation, Int. J. Pharm. 454 (2013) 462-471.

[66] D. Mou, H. Chen, J. Wan, H. Xu, X. Yang, Potent dried drug nanosuspensions for oral bioavailability enhancement of poorly soluble drugs with pH-dependent solubility, Int. J. Pharm. 413 (2011) 237-244.

[67] T. Heikkilä, H.A. Santos, N. Kumar, D.Y. Murzin, J. Salonen, T. Laaksonen, L. Peltonen, J. Hirvonen, V. Lehto, Cytotoxicity study of ordered mesoporous silica MCM-41 and SBA-15 microparticles on Caco-2 cells, Eur. J. Pharm. Biopharm. 74 (2010) 483-494.

List of Tables

FIGURE LEGENDS

Figure 1. Snapshots showing the location of the drug molecule in A. BEA and B. MCM framework every 40ps during the simulation run. C. Root mean squared displacement for KAZ3 in BEA and MCM-41.

Figure 2. Jetting images i) micro-dripping ii) unstable jetting iii) stable cone jet iv) stable multi-jet and jetting maps of **A.** SBA-15 in acetone **B.** SBA-15 in ethanol **C.** MCM-41 in acetone **D.** MCM-41 in ethanol **E.** FS in acetone and **F.** FS in ethanol.

Figure 3. Scanning electron microscope images of **A.** and **B**. SBA-15 at 5 kX and 40 kX magnification, respectively. **C**. and **D**. SBA-Eth-SIM at 5 kX and 40 kX magnification, respectively. **E**. and **F**. SBA-Eth-SP at 5 kX and 40 kX magnification, respectively. SBA: SBA-15, Eth: Ethanol, SIM: solvent impregnation method and SP: electrospraying method.

Figure 4. XRD patterns A., B., C. of pristine silica materials and the drug loaded formulations. D., E., F. DSC thermograms of SBA-15, MCM-41 and fumed silica-based formulations, SBA: SBA-15, MCM: MCM-41, FS: fumed silica, Eth: Ethanol, AC: acetone, SIM: solvent impregnation method and SP: electrospraying method.

Figure 5. Plots of θ^{o} values versus time for **A.** SBA-15, **B**. MCM-41 and **C**. FS before and after drug loading and **D**. digital images captured at different time intervals. SBA: SBA-15, MCM: MCM-41, FS: fumed silica, Eth: Ethanol, AC: acetone, SIM: solvent impregnation method and SP: electrospraying method.

Figure 6. *In vitro* release profiles of pure KAZ3 and KAZ3 loaded silica particles **A.** SBA-15, **B.** MCM-41 and **C**. FS using different solvents and loading methods (n=3). SBA: SBA-15, MCM: MCM-41, FS: fumed silica, Eth: Ethanol, AC: acetone, SIM: solvent impregnation method and SP: electrospraying method.

Figure 7. *Ex vivo* permeation profiles of plain drug and drug loaded in **A**. SBA-15, **B**. MCM-41 and **C.** FS particles using the non-everted sac method in Krebs-Ringer solution at 37 ^{o}C (n=3-5). SBA: SBA-15, MCM: MCM-41, FS: fumed silica, Eth: Ethanol, AC: acetone, SIM: solvent impregnation method and SP: electrospraying method.

Figure 8. A. Assessment of cell viability of Caco-2 cells exposed to KAZ3 (n=3). The cellular viability of Caco-2 cell cultures without treatment (negative control), after treatment with 1 % Triton X-100 (positive control) and after incubation with 0.1 mg/mL and 1 mg/mL of KAZ3-loaded MCM-41, SBA-15 and FS materials, for **B.** 4 h, **C**. 24 h and **D.** 48h was assessed by MTT assay (n=3). Eth: Ethanol, AC: acetone, SIM: solvent impregnation method and SP: electrospraying method.

Table 1. Quantification of KAZ3 encapsulation efficiency (EE %) of the different formulations calculated by UV spectrophotometry and TGA.

Formulation	MS type	Loading Method	Solvent	EE (%)-UV	EE (%)-TGA			
					Silica wt. loss (%) (100 °C-800 °C)	Formulation wt. loss (%) (100 °C-800 °C)	KAZ3 content (%)	EE (%)
SBA-AC-SIM	SBA-15	Solvent impregnation	Acetone	35.65 ± 3.25	8.23	25.7	17.47	69.88
SBA-Eth-SIM	SBA-15	Solvent impregnation	Ethanol	18.29 ± 0.86	8.23	24.29	16.06	64.25
SBA-AC-SP	SBA-15	EHDA	Acetone	114.53 ± 5.25	8.23	41.29	33.06	132.26
SBA-Eth-SP	SBA-15	EHDA	Ethanol	91.79 ± 0.42	8.23	34.75	26.52	106.10
MCM-AC-SIM	MCM-41	Solvent impregnation	Acetone	28.53 ± 0.73	14.8	29.33	14.53	58.13
MCM-Eth-SIM	MCM-41	Solvent impregnation	Ethanol	15.28 ± 10.28	14.8	29.91	15.11	60.45
MCM-AC-SP	MCM-41	EHDA	Acetone	105.89 ± 5.05	14.8	41.15	26.35	105.41
MCM-Eth-SP	MCM-41	EHDA	Ethanol	90.58 ± 0.72	14.8	32.3	17.50	70.0
FS-AC-SIM	Fumed silica	Solvent impregnation	Acetone	13.14 ± 2.95	8.16	27.34	19.18	76.72
FS-Eth-SIM	Fumed silica	Solvent impregnation	Ethanol	9.48 ± 0.38	8.16	29.24	21.24	84.98
FS-AC-SP	Fumed silica	EHDA	Acetone	115.18 ± 7.68	8.16	36.72	28.72	114.89
FS-Eth-SP	Fumed silica	EHDA	Ethanol	65.35 ± 0.37	8.16	29.42	21.42	85.71

Table 2. Apparent permeability (P_{app}) and steady state flux **(**J_{ss}**)** values of KAZ3 from different formulations using the non-everted intestinal sac method (n=3-5).

Sample	J_{ss} (ng/min/cm^2)	$P_{app} \cdot 10^{-7}$ (cm/s)	Enhancement Ratio
KAZ3 suspension	0.22 ± 0.02	8.88 ± 0.8	1
SBA-Eth-SIM	0.21 ± 0.07	8.32 ± 2.8	0.9
SBA-Eth-SP	0.63 ± 0.03	25.30 ± 1.2	2.8
MCM-Eth-SIM	0.09 ± 0.01	3.60 ± 0.4	0.4
MCM-Eth-SP	2.10 ± 0.02	84.0 ± 0.8	9.45
FS-Eth-SIM	0.31 ± 0.01	12.5 ± 0.40	1.4
FS-Eth-SP	0.83 ± 0.01	33.2 ± 0.39	3.7

FIGURE 1

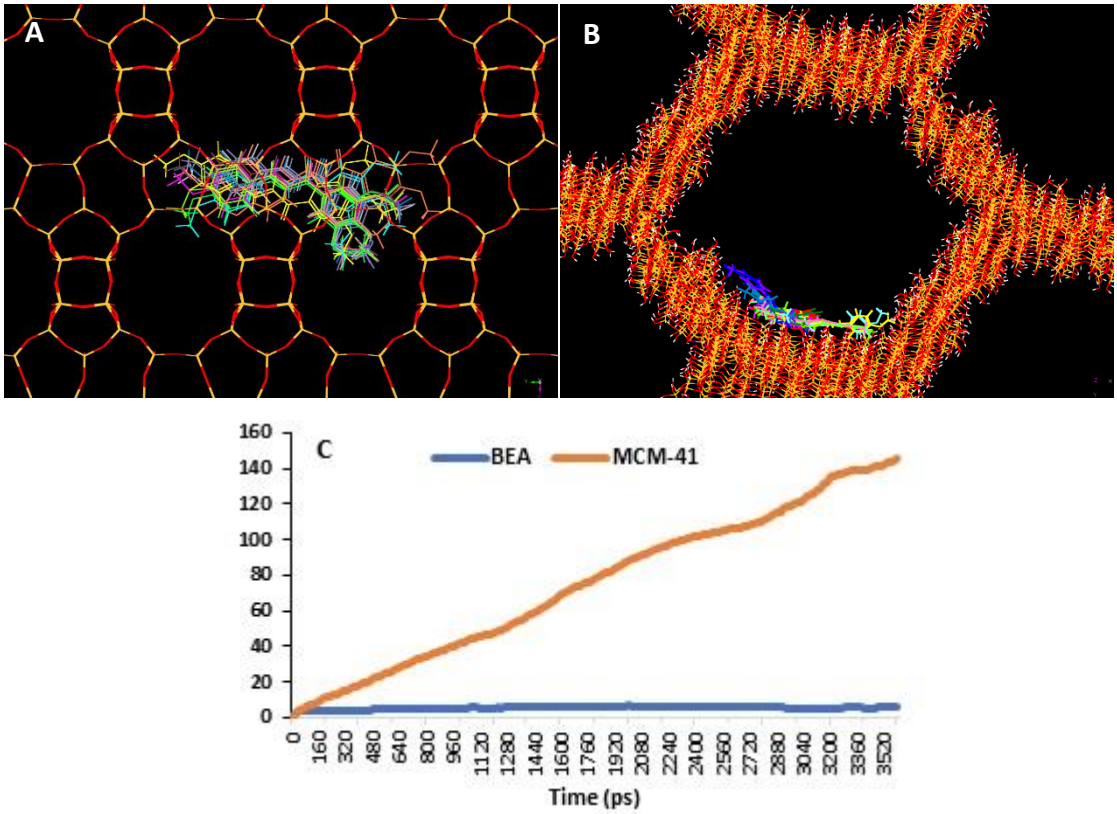
A
B
C
BEA
MCM-41
160
140
120
100
80
60
40
20
0
0
160
320
480
640
800
960
1120
1280
1440
1600
1760
1920
2080
2240
2400
2560
2720
2880
3040
3200
3360
3520
Time (ps)

FIGURE 2

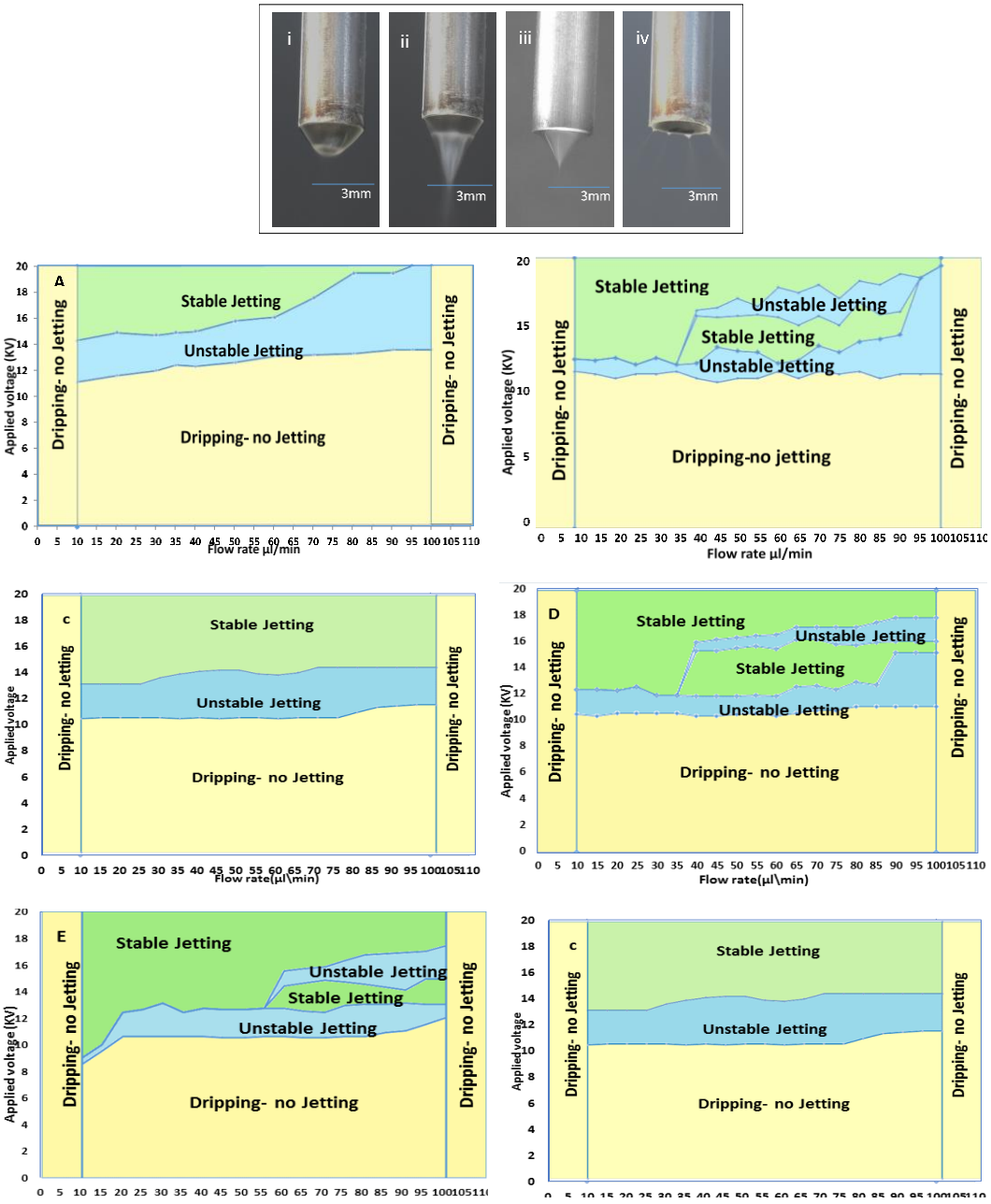
i
ii
iii
iv
3mm
A
Stable Jetting
Unstable Jetting
Dripping- no Jetting
Dripping- no Jetting
Dripping- no Jetting
Applied voltage (KV)
Flow rate µl/min
Stable Jetting
Unstable Jetting
Stable Jetting
Unstable Jetting
Dripping-no jetting
Dripping- no Jetting
Dripping- no Jetting
Applied voltage (KV)
Flow rate µl/min
C
Stable Jetting
Unstable Jetting
Dripping- no Jetting
Dripping- no Jetting
Dripping- no Jetting
Applied voltage
Flow rate(µl\min)
D
Stable Jetting
Unstable Jetting
Stable Jetting
Unstable Jetting
Dripping- no Jetting
Dripping- no Jetting
Dripping- no Jetting
Applied voltage (KV)
Flow rate(µl\min)
E
Stable Jetting
Unstable Jetting
Stable Jetting
Unstable Jetting
Dripping- no Jetting
Dripping- no Jetting
Dripping- no Jetting
Applied voltage (KV)
C
Stable Jetting
Unstable Jetting
Dripping- no Jetting
Dripping- no Jetting
Dripping- no Jetting
Applied voltage

FIGURE 3

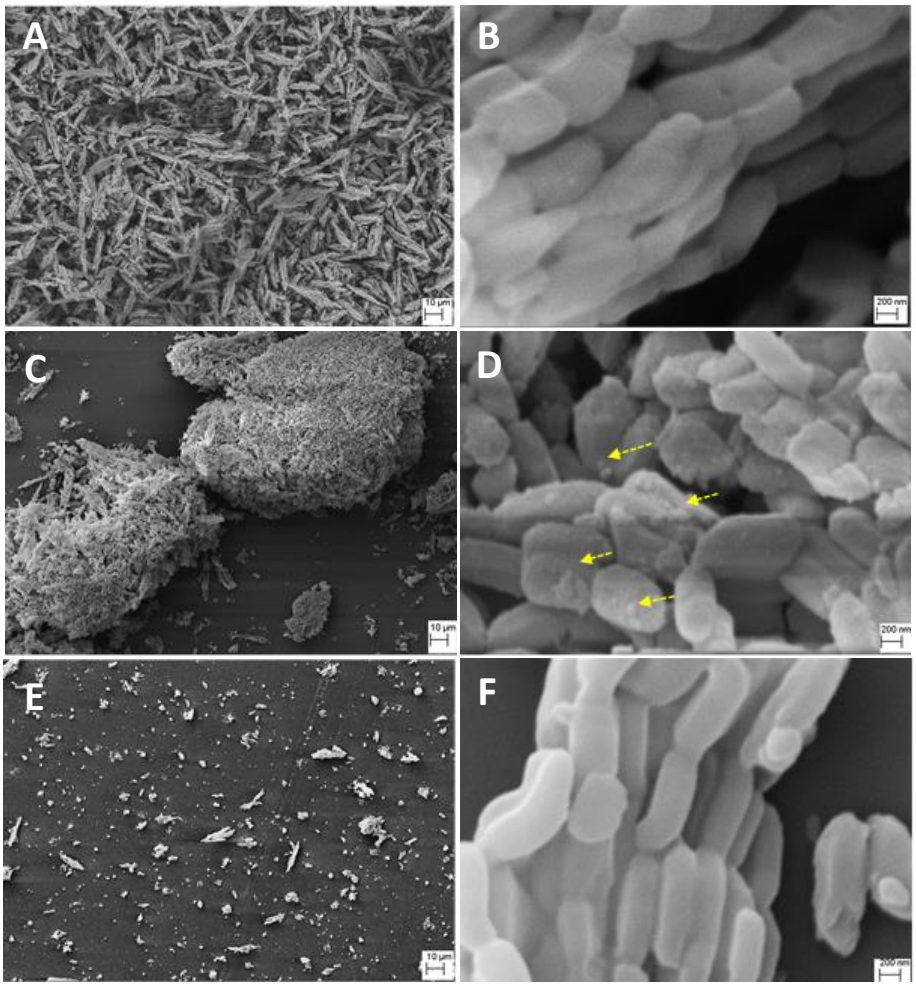

FIGURE 4

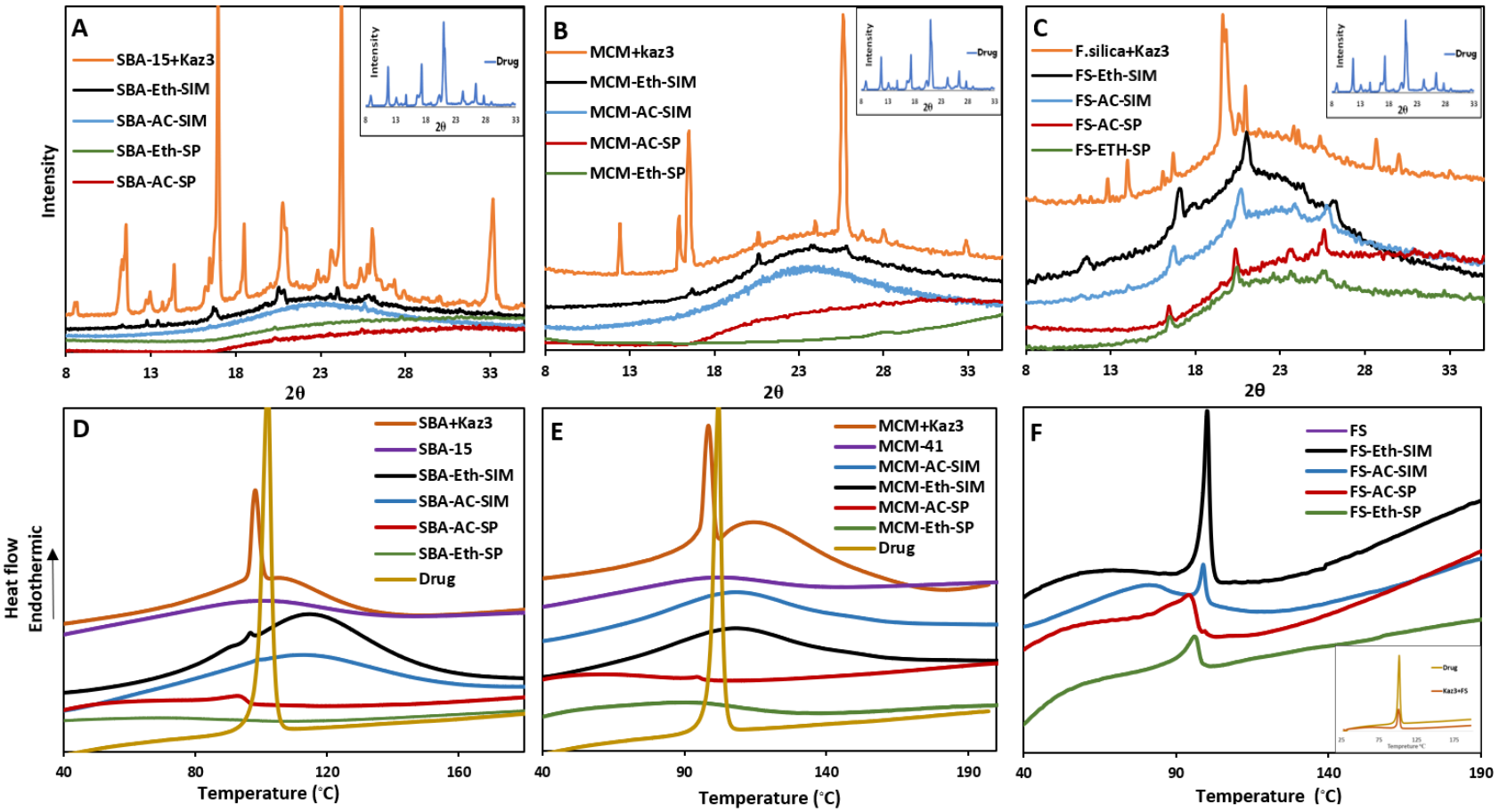
A
SBA-15+Kaz3
SBA-Eth-SIM
SBA-AC-SIM
SBA-Eth-SP
SBA-AC-SP
Intensity
2θ
B
MCM+kaz3
MCM-Eth-SIM
MCM-AC-SIM
MCM-AC-SP
MCM-Eth-SP
C
F.silica+Kaz3
FS-Eth-SIM
FS-AC-SIM
FS-AC-SP
FS-ETH-SP
D
SBA+Kaz3
SBA-15
SBA-Eth-SIM
SBA-AC-SIM
SBA-AC-SP
SBA-Eth-SP
Drug
Heat flow
Endothermic
Temperature (°C)
E
MCM+Kaz3
MCM-41
MCM-AC-SIM
MCM-Eth-SIM
MCM-AC-SP
MCM-Eth-SP
Drug
F
FS
FS-Eth-SIM
FS-AC-SIM
FS-AC-SP
FS-Eth-SP

FIGURE 5

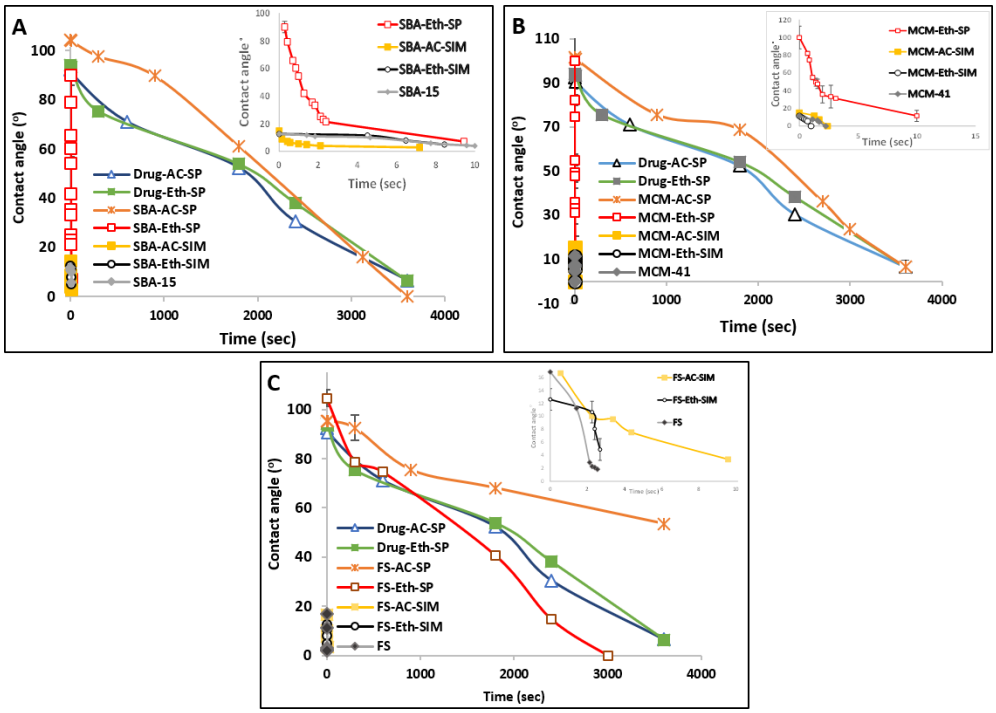
A
Contact angle (°)
Time (sec)
Drug-AC-SP
Drug-Eth-SP
SBA-AC-SP
SBA-Eth-SP
SBA-AC-SIM
SBA-Eth-SIM
SBA-15
B
Contact angle (°)
Time (sec)
Drug-AC-SP
Drug-Eth-SP
MCM-AC-SP
MCM-Eth-SP
MCM-AC-SIM
MCM-Eth-SIM
MCM-41
C
Contact angle (°)
Time (sec)
Drug-AC-SP
Drug-Eth-SP
FS-AC-SP
FS-Eth-SP
FS-AC-SIM
FS-Eth-SIM
FS

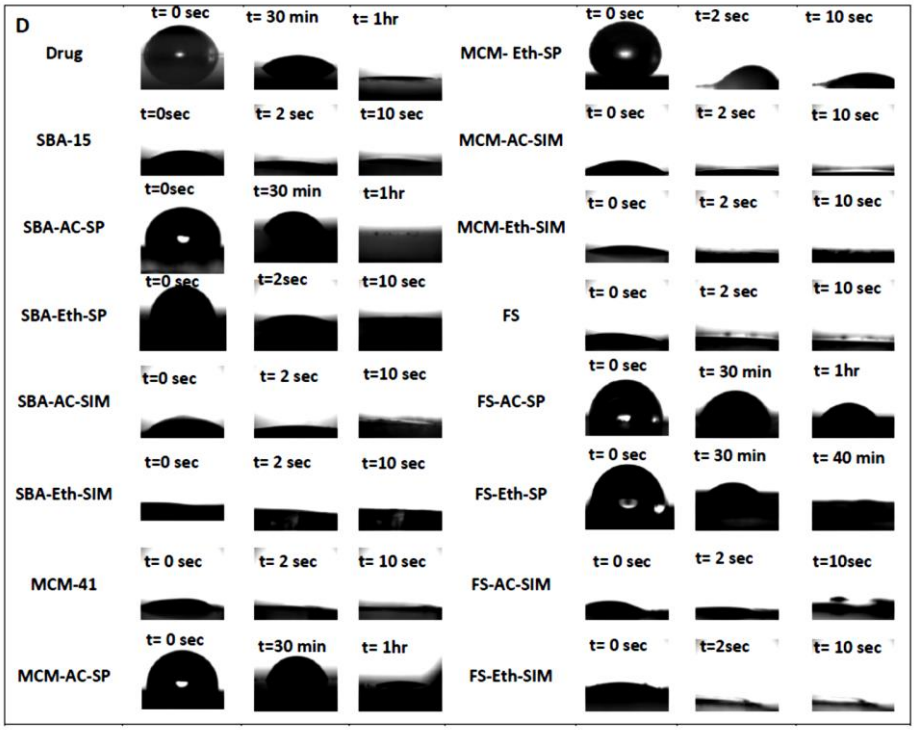
D
Drug
t= 0 sec
t= 30 min
t= 1hr
t=0sec
t= 2 sec
t=10 sec
SBA-15
t=0sec
t=30 min
t=1hr
SBA-AC-SP
t=0 sec
t=2sec
t=10 sec
SBA-Eth-SP
t=0 sec
t= 2 sec
t=10 sec
SBA-AC-SIM
t=0 sec
t= 2 sec
t=10 sec
SBA-Eth-SIM
t= 0 sec
t= 2 sec
t= 10 sec
MCM-41
t= 0 sec
t=30 min
t= 1hr
MCM-AC-SP
MCM- Eth-SP
t= 0 sec
t=2 sec
t= 10 sec
MCM-AC-SIM
t= 0 sec
t= 2 sec
t= 10 sec
MCM-Eth-SIM
t= 0 sec
t= 2 sec
t= 10 sec
FS
t= 0 sec
t= 30 min
t= 1hr
FS-AC-SP
t= 0 sec
t= 30 min
t= 40 min
FS-Eth-SP
t= 0 sec
t= 2 sec
t=10sec
FS-AC-SIM
t= 0 sec
t=2sec
t= 10 sec
FS-Eth-SIM

FIGURE 6

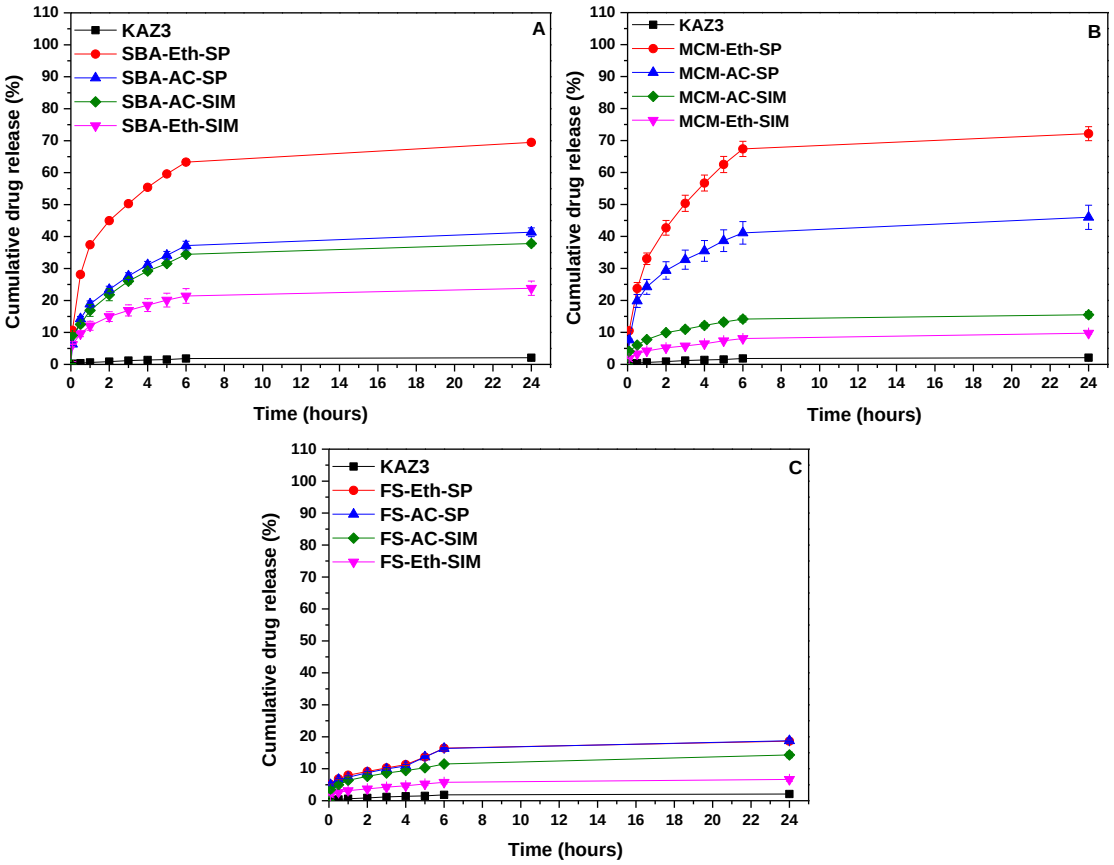
A
KAZ3
SBA-Eth-SP
SBA-AC-SP
SBA-AC-SIM
SBA-Eth-SIM
Cumulative drug release (%)
Time (hours)
B
KAZ3
MCM-Eth-SP
MCM-AC-SP
MCM-AC-SIM
MCM-Eth-SIM
Cumulative drug release (%)
Time (hours)
C
KAZ3
FS-Eth-SP
FS-AC-SP
FS-AC-SIM
FS-Eth-SIM
Cumulative drug release (%)
Time (hours)

FIGURE 7

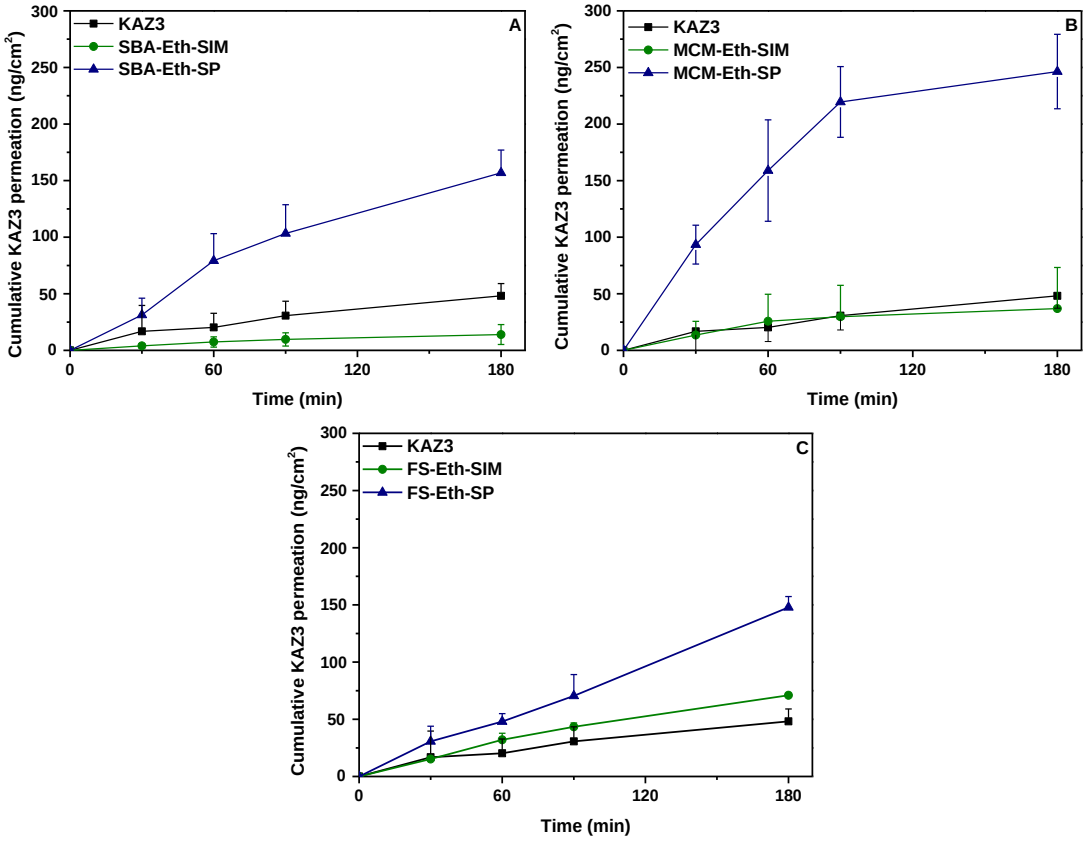
A
KAZ3
SBA-Eth-SIM
SBA-Eth-SP
Cumulative KAZ3 permeation (ng/cm²)
Time (min)
B
KAZ3
MCM-Eth-SIM
MCM-Eth-SP
Cumulative KAZ3 permeation (ng/cm²)
Time (min)
C
KAZ3
FS-Eth-SIM
FS-Eth-SP
Cumulative KAZ3 permeation (ng/cm²)
Time (min)

FIGURE 8

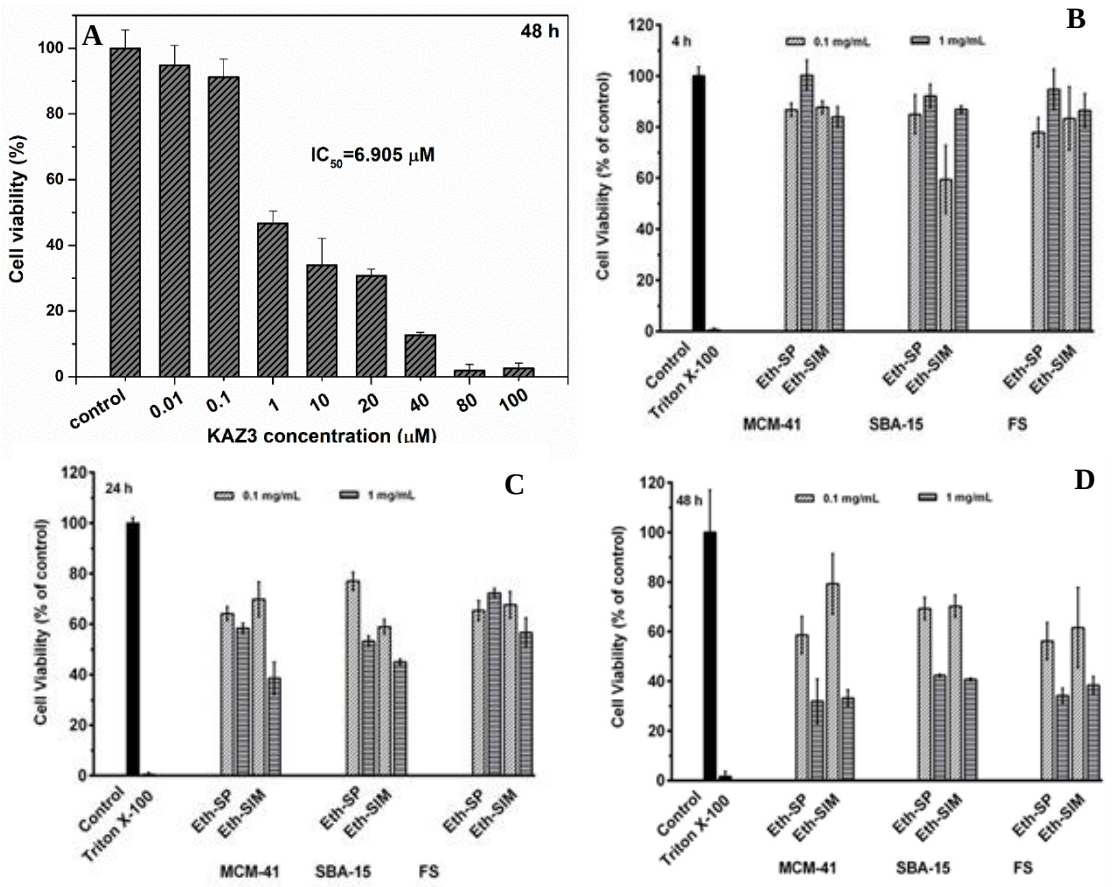
A
48 h
Cell viability (%)
IC50=6.905 μM
control
0.01
0.1
1
10
20
40
80
100
KAZ3 concentration (μM)
B
4 h
0.1 mg/mL
1 mg/mL
Cell Viability (% of control)
Control
Triton X-100
Eth-SP
Eth-SIM
MCM-41
SBA-15
FS
C
24 h
D
48 h